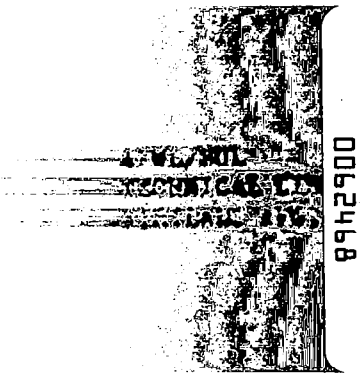

NASA Contractor Report 3665

Comparison of Forward Flight Effects Theory of A. Michalke and U. Michel With Measured Data

John W. Rawls, Jr.

CONTRACT NAS1-16000
JANUARY 1983

NASA

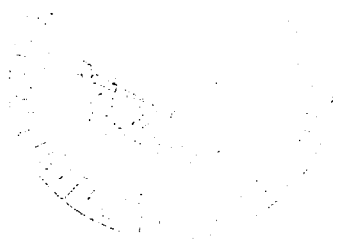

NASA Contractor Report 3665

Comparison of Forward Flight Effects Theory of A. Michalke and U. Michel With Measured Data

John W. Rawls, Jr.
Kentron International, Inc.
Hampton, Virginia

Prepared for
Langley Research Center
under Contract NAS1-16000

National Aeronautics
and Space Administration

**Scientific and Technical
Information Branch**

1983

TABLE OF CONTENTS

SUMMARY

The forward flight effects theory of A. Michalke and U. Michel is based on a far field solution to Lighthill's wave equation. This method is computationally effective with static jet noise prediction methods and is applicable to both single stream and dual stream jets. Comparisons are presented of the Michalke and Michel theory with measured flyover data. The results show that for shock free jets, the Michalke and Michel theory can successfully predict the effects of flight on the Overall Sound Pressure Level and the one-third octave band spectra.

INTRODUCTION

When a noise source is placed in motion, the fluctuations of the mean square pressure are altered from that of a stationary source. Simple sources in motion, such as monopoles, have been studied and are fairly well explained by classical results. The fluctuations of the mean square pressure of a jet, however, are not simple sources, but rather a random combination of many different types of sources. Lighthill was able to relate the noise generated by the turbulence in the mixing region of a static jet to that of a predominately quadrupole source, from which he derived the U^8 law (ref. 1). Ffowcs-Williams extended the theory to include forward motion of the aircraft, proposing that in-flight jets scale on the relative velocity (U_j-U_f)(ref. 2). It could be concluded, therefore, that a significant reduction in noise levels could be obtained by placing the jet in motion. Comparisons of this theory with data, however, showed an overprediction of the noise reduction in the forward arc.

The task of theoretically predicting the effects of motion on jet noise is a very complex one. An exact solution to the wave equation involving turbulence is virtually impossible. Even in the determination of flight effects experimentally, some degree of difficulty is encountered. Two types of testing are generally used in determining flight effects experimentally, full scale flyover tests and wind tunnel tests.

First, for flyover tests, the flight path of the aircraft must be carefully tracked. The noise that is emitted at point A by the jet, travels a distance r to the observer at the speed of sound a_0. Simultaneously, the aircraft moves from point A a distance equal to the aircraft velocity times the time it takes the sound to reach the observer or r/a_0. When the noise is heard by the observer, the aircraft is no longer at the point where the sound was emitted. For accurate data correlations it is essential to know where the aircraft was when the sound was emitted.

Atmospheric conditions such as temperature, humidity, wind speed and direction must be carefully monitored since they affect the attenuation of the noise signal. The jet noise component is often contaminated by other noise sources. For example, the spectra of high bypass turbofans are dominated by fan noise above 250 Hz. Ground effects, which are not yet fully understood, add still further complication in obtaining free field data.

Wind tunnels eliminate many of the problems associated with flyover data, since the testing takes place in a more controlled environment. Two types of wind tunnels are typically used to simulate the forward motion of the source, an anechoic tunnel and a free jet tunnel. In the anechoic tunnel, the microphones are placed in the tunnel flow. Consequently, flow effects over the microphone must be accounted for. In the free jet tunnel, on the other hand, the microphones are placed outside the mixing region of the free jet. The difficulty with the free jet tunnel arises in the reflection and refraction of the noise as it propagates through the shear layer. Both types of tunnels must be calibrated for background noise, to assure that the sound is properly absorbed by the tunnel walls.

Techniques have been developed to account for the reflection and refraction of the noise signal as it passes through the shear layer in free jets, enabling conversion of the data to in-flight conditions (ref. 3). The difficulty of tracking the aircraft in full scale testing was overcome by Drevet et al. (ref. 4) by placing a jet engine on a ground based vehicle. Thus, repeated runs could be made accurately and the average results reported.

The theoretical development of forward flight effects went virtually undocumented after 1963, when Ffowcs-Williams proposed his theory, until Michalke and Michel reexamined the problem in 1979 (refs. 5 and 6). The Michalke and Michel theory considers jet temperature effects. A theoretical model accounts for the stretching of the axial source length and uses static data to describe the effects of statistical properties in the far field instead of introducing a turbulence model. In 1980 the method was extended to coannular jets (ref. 7). In 1981 the theory was further extended to predict one-third octave band spectra for circular jets (ref. 8).

Although the Michalke and Michel theory was originally developed as a means of predicting forward flight effects from static tests, the method is ideally suited for uses with static jet noise prediction. For this reason, the theory has been compared with the Aerotrain data for possible use in the NASA Aircraft Noise Prediction Program (ANOPP). Two static jet noise prediction methods are used as a basis for the Michalke and Michel theory: the Society of Automotive Engineers (SAE) Aerospace Recommended Practice (ARP) Number 876 (refs. 9 and 10) and the J. R. Stone prediction method (ref. 11). Each of these methods uses empirical data to describe the directivity and spectral shapes as a function of relevant parameters. Each method also has a means of predicting forward flight effects.

SYMBOLS LIST

A	stretching parameter
a_f	apparent sound speed $a_o (1 - M_f \cos \theta_o)$
a_o	ambient sound pressure
B_F	$1 + .7\ U_e \cos \theta_o$
B_s	$\sigma\ (1. + .7\ \sigma\ U_e \cos \theta_o)$
D	jet diameter
F	source function
f	frequency
$\tilde{f}$	normalized frequency $\tilde{f} = fD/\Delta U$
K	normalization coefficient $K = \frac{(\rho_o a_o^2)^2\ D}{4\pi\ \tilde{r}_o^2\ \ a_o} \left(\frac{\rho_j}{\rho_o}\right)^2$
M_c	convected Mach number $.65\ U_j/a_o$
M_c'	convected flight Mach number $.65\ (U_j - U_f)/a_o$
M_f	aircraft Mach number U_f/a_o
OASPL	overall sound pressure level in dB relative to 20μ Pa.
ΔOASPL	$OASPL_{static} - OASPL_{flight}$
p	sound pressure
$\tilde{p}'$	normalized sound pressure $p'/(\rho_j\ \Delta U^2)$
$\langle p^2 \rangle$	mean square pressure in one-third-octave bands
q_1	Reynolds stress source term
q_2	pressure-density gradient source term

r	distance from source to observer
r_o	wave normal distance
$\tilde{r}_o$	normalized wave normal distance $\tilde{r}_o = r_o/D$
St	Strouhal number $St = fD/\Delta U$
St_s	equivalent static Strouhal number $St_s = St/\sigma$
T	temperature
t	time
U	velocity
U_e	equivalent static jet velocity $U_e = \Delta U/(1 - M_f \cos \theta_o)$
ΔU	$U_j - U_f$
W_{FF}	cross spectral density
$\tilde{W}_{FF}$	normalized cross spectral density
W_{WT}	power spectral density
x_i	observer location in far-field, i=1, 2, 3
y_i	source point location, i=1, 2, 3
$\tilde{y}_i$	normalized source location $\tilde{y}_i = y_i/D$
y_{s_i}	contracted source coordinate
β	correction factor to forward arc OASPL
δ	angle between flight vector and engine inlet axis
θ	angle between far-field point and nozzle measured from inlet axis
θ_o	emission angle wave normal direction

ρ	density
σ	stretching factor $\sigma = 1 + A \frac{U_f}{\Delta U}$
σ_I	ratio of normalized turbulent mean square values of F (flight/static)
τ	difference between retarded times
ψ_F	phase of the source function F
ψ_r	phase of the interference function

SUBSCRIPTS

a	ambient
e	effective
f	flight
FO	in flyover coordinates
j	jet exit condition
o	wave normal
r	retarded
r_o	component in wave normal direction
s	static; contracted
WT	in wind tunnel coordinates

SUPERSCRIPTS

$\overline{\quad}$	time average
~	normalized values

METHOD OF A. MICHALKE AND U. MICHEL FOR PREDICTING FLYOVER JET NOISE FROM STATIC TESTS

The forward flight effects noise prediction theory of A. Michalke and U. Michel for shock free circular jets is based on the solution of the convected Lighthill equation in the far field. The sound pressure for an observer at location x_i at time t as given in ref. 8 is

$$p'(x_i,t) = \frac{1}{4\pi r_o} \frac{a_o}{a_f^2} \left[\int F(y_i,t) \Big|_{t_r} dy_i \right] \tag{1}$$

where r_o is the wave normal distance, y_i is the source position, and a_o is the ambient speed of sound. The source function $F(y_i,t)$ is defined by

$$F(y_i,t) = \frac{1}{a_f} \frac{\partial^2 q_1}{\partial t^2} + \frac{\partial q_2}{\partial t} \tag{2}$$

where $\partial^2 q_1/\partial t^2$ represents a quadrupole source and $\partial q_2/\partial t$ represents a dipole source. The solution given in equation (1) is valid in a nozzle fixed coordinate system, where the source is assumed stationary with an external flow simulating the forward velocity. (Michalke and Michel refer to this with a subscript WT for wind tunnel coordinates.)

The apparent sound speed a_f, given by

$$a_f = a_o (1 - M_f \cos \Theta_o) \tag{3}$$

in this coordinate system, is the ambient sound speed plus the component of the flow velocity in the wave normal direction.

The integration of the source function $F(y_i,t)$ must be done at the time the sound is emitted, i.e. at the retarded time in the observer coordinates. The noise sources are randomly distributed throughout the mixing region, each having a unique location and a unique retarted time. The retarded time for a source located

at the origin is

$$t_r = t - \frac{r}{a_f} \tag{4a}$$

which in terms of the wave normal direction is

$$t_r = t - \frac{r_o}{a_o} \tag{4b}$$

since the time it takes the sound to travel the distance r in the presence of flow is the same amount of time it takes to travel the distance r_o without flow. For sources not located at the origin, an additional term must be added which is the component of the source location in the wave normal direction divided by the apparent sound speed, as shown in figure 1. The complete retarded time equation is

$$t_r = t - \frac{r_o}{a_o} + \frac{y_{r_o}}{a_f} \tag{4c}$$

In the nozzle fixed coordinate system, the jet mixing process is stationary random, i.e., the turbulence intensity is independent of time. The power spectral density of the pressure fluctuation in the far field is

$$W_{WT}(x_i,f) = \frac{a_o^2}{(4\pi r_o a_f^2)^2} \iint W_{FF}(y_i,n_i,f) \exp(-i2\pi f \Delta t_r)\, dn_i\, dy_i \tag{5}$$

where the cross spectral density is

$$W_{FF}(y_i,n_i,f) = \int_{-\infty}^{\infty} \overline{F(y_i,t)\, F(y_i + n_i,\, t+\tau)} \exp(i2\pi f\tau)\, d\tau \tag{6}$$

and the source function $F(y_i,t)$ is defined by equation 2. The exponential function in equation 5 is an interference function due to the retarded time difference between two source position separated by a distance n_i. The source function $F(y_i,t)$ is explicitly a function of the flight velocity as are the

integration volumes dn_i and dy_i. The approach of Michalke and Michel is to derive scaling laws which remove the flight dependence from inside the integration of equation 5, so that the effect of motion can be determined by a static jet.

Through the proper choice of normalization, Michalke and Michel show that the power spectral density can be written as

$$W_{WT}(x_i,f) = (1 - M_f \cos \theta_o) \left(\frac{U_e}{a_o}\right)^5 K \iint \tilde{W}_{FF} \exp(-i\psi_r)\, d\tilde{n}_i d\tilde{y}_i \tag{7}$$

where

$$\psi_r = 2\pi f \Delta t_r = 2\pi \tilde{f} \frac{U_e}{a_o} \tilde{n}_{r_o} \tag{8}$$

is the phase of the interference function and K is a normalization coefficient. (The normalized variables are defined in the symbols list.) As a result of the normalization, an effective velocity U_e is defined by

$$U_e = \frac{\Delta U}{1 - M_f \cos \theta_o} \tag{9}$$

which represents an equivalent static jet velocity as a function of emission angle.

The integrating volumes are, however, still a function of U_f due to the elongation of the jet mixing region. In order to eliminate this dependence, Michalke and Michel introduce a stretching model based on the assumption that a fluid particle in a static jet reaches the same amount of diffusion after the same time as a jet in flight, provided the relative velocity of the two jets are the same. The ratio of the mixing lengths of the in-flight jet to the static jet

defines the stretching factor σ given by

$$\sigma = 1 + A \frac{U_f}{\Delta U} \tag{10}$$

where A is a stretching parameter equal to 1.4.

The stretching factor defines a new coordinate system

$$\tilde{y}_{s_i} = \left(\frac{\tilde{y}_1}{\sigma}, \tilde{y}_2, \tilde{y}_3\right) \tag{11}$$

where the static jet axis is contracted. The stretching of the flight mixing length also reduces the equivalent static Strouhal number from the flight Strouhal number (ref. 12) by

$$St_s = \frac{St}{\sigma} \tag{12}$$

Since the flight dependence on the integration volume is not yet completely eliminated, the cross spectral density is written in terms of its magnitude and phase.

$$W_{FF} = \left| W_{FF} \right| \exp\left(i\psi_F\right) \tag{13}$$

Using (11) and (12) the magnitude of the cross spectral density in-flight can be related to the static cross spectral density by

$$\left|\tilde{W}_{FF}\left(St, y_i, \eta_i, \theta_o, \frac{U_j}{a_o}, M_f\right)\right| = \left| \tilde{W}_{FF}\left(St_s, \tilde{y}_{s_i}, \tilde{\eta}_{s_i}, \theta_o, \frac{U_e}{a_o}, 0\right) \right| \frac{\sigma_1}{\sigma} \tag{14}$$

The flight dependence on the magnitude of the cross spectral density can be eliminated if

one; the magnitude of the equivalent static cross spectral density is evaluated at the modified jet velocity defined by equation 8,

two; the magnitude of the equivalent static cross spectral density is evaluated in the contracted coordinate system defined by equation 10, and finally,

three; the magnitude of the equivalent static cross spectral density is evaluated at the modified Strouhol number defined by equation 11.

The term σ_1 is the ratio of the mean square value of $\tilde{F}$ in flight to the corresponding equivalent static jet. Michalke and Michel indicate that $\sigma_1 = \sigma$ is a good approximation, which means that the magnitude of the cross spectral density in flight is nearly independent of U_f when the static cross spectral density is evaluated with the proper set of parameters.

By using equation (11), the power spectral density can be determined by integrating equation (7) with

$$\tilde{dy}_i = \sigma \, \tilde{dy}_{s_i} \tag{15}$$

and

$$\tilde{d\eta}_i = \sigma \, \tilde{d\eta}_{s_i} \tag{16}$$

to yield with equation (14)

$$W_{WT}(\tilde{r}_o, \theta_o, St, \frac{U_j}{a_o}, M_f) = \sigma_1 \sigma (1 - M_f \cos \theta_o) \left(\frac{U_e}{a_o}\right)^5 KI_f \tag{17}$$

where

$$I_f = \iint \left| W_{FF}(St_s, \tilde{y}_{s_i}, \tilde{n}_{s_i}, \theta_o, \frac{U_e}{a_o}, 0) \right| \exp\left[i\Delta\psi\ (St, \tilde{y}_{s_i}, \tilde{n}_{s_i}, \theta_o) \right] d\tilde{n}_{s_i} d\tilde{y}_{s_i} \quad (18)$$

Here $\Delta\psi = \psi_F - \psi_r$.

If equations 17 and 18 are evaluated once in the flight case $(U_j/a_o, M_f)$ and once in the static case $(U_s/a_o, o)$, it can be seen that power spectral density in flight is related to the static power spectral density by the following equation

$$W_{WT}(\tilde{r}_o, \theta_o, St, \frac{U_j}{a_o}, M_f) = \sigma_1\sigma(1 - M_f\cos\theta_o)\ W_{WT}(\tilde{r}_o, \theta_o, St_s, \frac{U_e}{a_o}, 0) \quad (19)$$

if the static jet velocity is chosen as

$$\frac{U_s}{a_o} = \frac{U_e}{a_o} \quad (20)$$

In addition, it is assumed that the difference between $\Delta\psi\ (St, U_j/a_o, M_f)$ and $\Delta\psi\ (St_s, U_s/a_o, 0)$ is negligible. While the M_f-dependence of the magnitude of the cross-spectral density was eliminated through the normalization and the introduction of the stretching model, the elimination of the M_f dependence on the phase $\Delta\psi$ was not possible. It was pointed out in reference 8 that this omission may lead to an over-prediction of flight jet noise in the forward arc.

The solution for the power spectral density given in equation (18) is in terms of the wind tunnel coordinates. To transform to observer coordinates, or flyover coordinates, the observer point x_i is assumed to move with velocity U_f. As a result of this apparent motion, the observer Strouhal number St_o is Doppler shifted by

$$St_o = St(1 - M_f \cos \theta_o) \tag{21}$$

and the power spectral density in observer coordinates is related to the nozzle fixed coordinates by (Ref. 13).

$$W_{FO}(\tilde{r}_o, \theta_o, St, \frac{U_j}{a_o}, M_f) = (1 - M_f \cos \theta_o) W_{WT}(\tilde{r}_o, \theta_o, St, \frac{U_j}{a_o}, M_f) \tag{22}$$

Consequently, the power spectral density in flyover coordinates is given by

$$W_{FO}(\tilde{r}_o, \theta_o, St, \frac{U_j}{a_o}, M_f) = \sigma_1 \sigma (1 - M_f \cos \theta_o)^2 W_{FO}(\tilde{r}_o, \theta_o, St_{so}, \frac{U_e}{a_o}, 0) \tag{23}$$

where the equivalent static observer Strouhal number St_{so} is given by

$$St_{so} = \frac{St}{\sigma} (1 - M_f \cos \theta_o) \tag{24}$$

In terms of one-third-octave band spectra, the mean square pressure is obtained by integrating equation (20) between the limits $f_1 = \sigma f_{s_1}$ and $f_2 = \sigma f_{s_2}$

$$\langle P^2 \rangle_{FO}(\tilde{r}_o, \theta_o, St_c, \frac{U_j}{a_o}, M_f) = \sigma_1 \sigma^2 (1 - M_f \cos \theta_o)^2 \langle P^2 \rangle_{FO}(\tilde{r}_o, \theta_o, St_c \frac{(1 - M_f \cos \theta_o)}{\sigma}, \frac{U_e}{a_o}, 0) \tag{25}$$

where

$$St_c = \frac{f_c D}{\Delta U} \tag{26}$$

and f_c is the one-third-octave band center frequency.

The effects of flight on 1/3 octave band mean square pressure can be scaled to a static jet by equation (25) if the static jet is evaluated at the modified Strouhal number, defined by

$$St_s = \frac{f_{cs}D}{U_e} = \frac{f_cD}{U_e\sigma} = St_c \frac{(1 - M_f\cos\theta_o)}{\sigma} \tag{27}$$

and the equivalent jet velocity defined by

$$U_e = \frac{U_j - U_f}{(1 - M_f \cos\theta_o)} \tag{28}$$

The results of the scaling laws in equation 25 are a factor of

i. σ caused by the increased source length
ii. σ caused by the increased coherence length
iii. σ_1 caused by the increased normalized turbulence fluctuations
iv. $(1 - M_f \cos\theta)$ as a result of the normalization
v. $(1 - M_f \cos\theta)$ caused by the transformation to flyover coordinates

SAE ARP-876

JET NOISE PREDICTION METHOD

The Society of Automotive Engineers (SAE) Aerospace Recommended Practice (ARP) Number 876 method predicts single stream jet mixing noise from shock free circular nozzles. The ratio of mean square pressure inflight to the mean square pressure in the static case is

$$\frac{\langle p^2 \rangle_{flight}}{\langle p^2 \rangle_{static}} = \frac{1}{1 - M_f \cos(\theta - \delta)} \left[\frac{U_j - U_f}{U_j} \right]^{m(\theta)} \tag{29}$$

where δ is the angle between the flight vector and the engine inlet axis and $m(\theta)$ is a flight index function. The first term on the right hand side of equation (28) is the convective amplification of the static directivity function while the second term is an empirical function to account for all other flight effects. The ARP-876 method, which technically is only the static prediction, is widely accepted as a means of predicting circular jet noise. Each member of the International Civil Aviation Organization (ICAO) committee (Table 1) uses the ARP-876 method, however, each has their own modification of the index function. The index function $m(\theta)$ used in ANOPP is given in Table 2.

The Strouhal Number is not Doppler shifted with this method but is based on the relative velocity

$$St = \frac{fD}{(U_j - U_f)} \tag{30}$$

J. R. STONE PREDICTION METHOD

Stone's jet noise prediction method predicts the far-field mean-square acoustic pressure for single stream and coaxial nozzle jets. The ratio of the mean square pressure (flight to static) is given by

$$\frac{\langle p^2 \rangle_{flight}}{\langle p^2 \rangle_{static}} = \left[\begin{array}{c}\text{KINEMATIC}\\ \text{EFFECTS}\end{array}\right] \left[\begin{array}{c}\text{DYNAMIC}\\ \text{EFFECTS}\end{array}\right] \left[\begin{array}{c}\text{SOURCE STRENGTH}\\ \text{ALTERATION}\end{array}\right] \tag{31}$$

The kinematic effects are a convective amplification of the source directivity given by

$$\left[\begin{array}{c}\text{KINEMATIC}\\ \text{EFFECTS}\end{array}\right] = \frac{1}{1 - M_f \cos(\theta_o - \delta)} \tag{32}$$

where δ is the angle between the flight vector and the engine inlet axis.

The dynamic effects are given by

$$\left[\begin{array}{c}\text{DYNAMIC}\\ \text{EFFECTS}\end{array}\right] = \left[\frac{(1 + M_c' \cos\theta_o)^2 + (\alpha M_c')^2}{(1 + M_c \cos\theta_o)^2 + (\alpha M_c)^2}\right]^{-3/2} \tag{33}$$

where M_c is the convective Mach number

$$M_c = .65(U_j/a_o) \tag{34}$$

and M_c' is the convective Mach number based on the relative velocity

$$M_c' = .65(U_j - U_f)/a_o \tag{35}$$

The turbulent length scale ratio α is 0.2.

The source strength alteration is given by

$$\left[\begin{array}{c}\text{SOURCE STRENGTH} \\ \text{ALTERATION}\end{array}\right] = \left(\frac{1 - U_f}{U_j}\right)^5 \left(\frac{\rho_j}{\rho_a}\right)^{\omega} \tag{36}$$

where

$$\omega = \frac{3\ M_c^{3.5}}{.6 + M_c^{3.5}} - 1 \tag{37}$$

and where

$$M_c = \frac{U_j}{a_o}\left[1 - \frac{U_f}{U_j}\right]^{2/3} \tag{38}$$

The Strouhal number given by

$$St = \frac{fD}{U_j - U_f}\left[1 - M_f \cos\left(\theta_o - \delta\right)\right]\left[\frac{T_j}{T_a}\right]^{.4(1 + \cos\theta')}$$

$$x \left[\frac{(1 + M_c' \cos\theta_o)^2 + (\alpha\ M_c')^2}{(1 + M_c \cos\theta_o)^2 + (\alpha\ M_c)^2}\right]^{1/2} \tag{39}$$

is Doppler shift with an additional correction for temperature and convection effects and where θ' is a function of the jet velocity given by

$$\theta' = \theta_o\ (U_j/a_o)^{.1} \tag{40}$$

COMPARISON OF THEORY WITH EXPERIMENTAL DATA

Since the forward motion of the noise source affects both the overall sound pressure level and the one-third octave band spectra, predictions have been compared with measured data for each. Further, because the accuracy of the flight prediction depends to a large extent on the accuracy of the static prediction, two separate static jet noise predictions are used to compare theory with measured data. The two static prediction methods used are the SAE ARP-876 method and the J. R. Stone method. Each of the methods are programmed in the NASA Aircraft Noise Prediction Program (ANOPP).

In this report, prediction of the Michalke and Michel theory using the ARP-876 method will be indicated by MM/ARP-876. Similarly, prediction of the Michalke and Michel theory using the Stone static prediction method will be indicated by MM/Stone.

The Overall Sound Pressure Level results are presented as the relative overall sound pressure level defined by

$$\Delta OASPL = OASPL_{static} - OASPL_{flight} \tag{41}$$

The implication of this presentation is that values greater than zero indicate a noise reduction (below the static level) and values less than zero indicate a noise increase (above the static level).

The one-third octave band spectra are also presented on a relative basis as SPL-OASPL. The fly-over and static spectra are compared at emission angles of 30°, 60°, 90°, 120° and 150°.

Data Base

The Bertin Aerotrain data used to compare with the theory were obtained from SNECMA and the study conducted by Drevet, Duponchel and Jacques (ref. 4). Data were collected using a GE J85 engine mounted on the Aerotrain. The nozzle is a

convergent type with a diameter of .293 meters. The directivity and spectra have been corrected to standard day conditions (ISA +10°C and 70% relative humidity) and ground reflections. The data are presented relative to a sideline distance of 50 meters with angular dependence relative to the nozzle inlet axis.

Five jet velocities are included in the data set ranging from V_j/a_0 = 1.09 to V_j/a_0 = 1.84. Table III gives the operating conditions for each case. The simulated flight Mach number in all cases is .24.

Overall Sound Pressure Level

Results Figure 2 shows the relative OASPL prediction using the theory of Michalke and Michel and the relative ARP-876 prediction compared with measured data. The minimum flight effect appears to be independent of the jet velocity, occurring at an emission angle between 60° and 70° in all five cases. One might have expected the minimum flight effect to occur at 90°; however, both the MM/ARP-876 prediction and the ARP-876 prediction, as well as the data, confirm this report.

At 90°, the data indicates a noise reduction of approximately 1.5 dB in case 1, which decrease in cases 2 and 3 with an increase in the jet velocity. In cases 4 and 5, the jet velocity has increased sufficiently so that there is virtually no noise reduction at 90°. The MM/ARP-876 prediction agrees very well with the data in case 1, 2 and 3. However, in cases 4 and 5, the Michalke and Michel theory predicts an increase in the noise reduction at 90° with increasing jet velocity rather than a decrease as indicated by the data.

The MM/ARP-876 prediction of the forward arc is characterized by a forward arc amplification of approximately 3 dB at 30°. The agreement with the data is very good in case 1 and 2. Michalke and Michel report in ref. 8 that an over prediction of the forward arc may be expected due to the omission of the retarded time difference between two source points. This is apparent in cases 3 and 4. In case 5, the Michalke and Michel theory again agrees with the data. However, since the pressure

ratio in this case is well into the supercritical range, this may be a result of shock noise contamination masking the true jet noise effects.

The Michalke and Michel prediction of the aft arc agrees very well with the data in cases 1 through 4. In case 5, the Michalke and Michel theory underpredicts the noise level by 2.5 dB at 130°.

In general, the ARP-876 method demonstrates good correlations with the data at all angles. This is not surprising since the flight index function $m(\Theta)$ was derived using the Bertin Aerotrain data.

Figure 3 shows the same comparison as figure 2; however, Stone's method has been substituted for the ARP-876 method. In general the same trend holds concerning the Michalke and Michel using Stone's method as was discussed using the ARP-876 method. Stone's method does not predict a forward amplification and therefore does not compare well with this data.

Discussion In order to determine the cause of the underprediction of the flight OASPL at 90° using the Michalke and Michel theory, the equation for the relative OASPL is examined. At 90°, ΔOASPL is given by

$$\Delta\text{OASPL} = \text{OASPL}\ (U_j/a_o) - \text{OASPL}\ (\Delta U/a_o) - 10\ \text{Log}\ \sigma_1 - 20\ \text{Log}\ \sigma \qquad (42)$$

In order to increase the flight OASPL, either the stretching factor σ or the turbulence factor σ_1 must increase. Reasonable values of the stretching parameter A, as indicated in ref 6 are between 1 and 3. This will improve the prediction agreement with data at 90° and in the aft arc but cause the forward arc to be over predicted.

Alternatively, since the pressure ratios are supercritical in cases 4 and 5 it may be speculated that the turbulent structure changes in such a way that the

noise level is increased at 90°. If this is true, then σ_1 may no longer equal σ in the region where the pressure ratio is supercritical.

The two parameters in the Michalke and Michel theory which may be adjusted are the stretching parameter A, which has been experimentally determined to be 1.4 and σ_1 the ratio of the flight to static turbulence intensity. Changing the stretching factor will directly increase or decrease the flight OASPL.

The agreement with the data at 90° is good when $U_j/a_o \leq 1.5$. When U_j/a_o is increased above 1.5, the Michalke and Michel tends to underpredict the noise level at 90°. An increase in the stretching factor will improve the data-theory correlation in these cases. However an increase in the stretching parameter will also cause the flight spectra to be shifted in the high frequency direction and, therefore, no adjustment to the stretching parameter is desirable.

An adjustment to the turbulence factor σ_1 does seem in order for the cases where $U_j/a_o > 1.5$. If the flight OASPL is adjusted to agree with the data at 90°, the aft arc prediction is significantly improved (figure 4). This will cause the forward arc to be over predicted and thus will require an additional correction. This seems reasonable to expect since an over prediction of the forward arc is anticipated by the influence of M_f on the phase difference in the source integral.

An alteration to the forward arc was proposed by U. Michel of the following form

$$\beta = 10 \text{ Log } \frac{B^2 + B_s^2}{B^2 + B_F^2} \tag{43}$$

where

$$B_s = 1 + .7 U_e \cos\theta \tag{44}$$

and

$$B_F = \sigma(1 + .7\sigma U_e \cos\theta_o) \tag{45}$$

and where B has been chosen to be 4. If this adjustment is applied to the theory using the ARP-876 method, along with an adjustment of the level at 90° and applied only to cases 3, 4 and 5 where $U_j/a_0 > 1.5$, the agreement with the data is significantly improved (figure 5). This seems to indicate that the basic theory is correct, but some empirical enhancement is necessary, especially in the determination of σ_1 for normalized jet velocity in the range of 1.5 and larger.

The prediction of forward flight effects, like most other aeroacoustic prediction methods, has developed along two paths, the empirical methods and the theoretical methods. Empirical methods can be developed with relative ease, given sufficient data. Unfortunately they yield little in the way of explaining the mechanism which causes a particular phenomenon to occur. They are also generally limited to a specific application. The index method used in the ARP-876 method is limited to circular nozzles.

The Michalke and Michel theory however is easily extended to coaxial nozzles. Figure 6 shows the theory using Stone's coaxial prediction method as a basis to compare with data from a Rolls Royce RB-211 high bypass turbofan engine. This data was obtained in a flyover test with the engine mounted on a VC-10 aircraft (Ref. 14). Since the 1/3 octave band spectra above 250 Hz is dominated by the noise, the jet noise is assumed to be the sum of the 1/3 octave band spectra from 50 to 250 Hz.

The ΔOASPL values are correctly predicted by the Michalke and Michel theory in the cases 4 and 5 for a flight Mach number $M_f = 0.27$. The agreement is equally well in case 3 where $M_f = 0.50$. No airframe noise contamination can be recognized. The cases 1 and 2 demonstrate higher ΔOASPL values in the predictions than in the measurements. This can be explained with airframe noise in case 2 where slats and 20° flaps were deployed. The good agreement in the cases 3, 4, and 5 show promise for the use of the theory with coaxial jets.

One-third Octave Band Spectra

Results Upon examination of the MM/ARP-876 prediction of the one-third octave band spectra in figures 7a - 11a and the MM/Stone prediction in figures 12a - 16a, two significant differences can be identified. First, the MM/ARP-876 prediction at 30° and 60° for all jet velocities is shifted in the high frequency direction from the data. At 30°, this shift is approximately one-octave band and at 60° approximately one-third octave band. The MM/Stone prediction also is shifted toward the high frequency range, but much less so than the Michalke and Michel prediction using the ARP-876 method.

Second, the shape of the MM/ARP-876 spectra at 150° for $U_j/a_0 = 1.63$ (fig. 10a) is quite different from the data. The MM/Stone prediction for the same case (fig. 15a) shows very good agreement with the data.

Discussion In order to determine if the shift of the Michalke and Michel spectra (using the ARP-876 method) is due to the theory or to the static prediction method, one must look at the static spectra. Comparison of the ARP-876 static prediction with data are shown in figures 7b through 11b. In general the ARP-876 static predictions at 30° and 60° are also shifted in the high frequency direction, which will account in part for the shift of the Michalke and Michel flight spectra. The spectrum at 30° and $U_j/a_0 = 1.29$ in figure 8a is determined from a static jet with a velocity $U_e/a_0 = 1.63$. The corresponding static ARP-876 prediction is plotted in figure 10b. One will realize that the difference between this prediction and the measured data is very similar to the difference between the Michalke and Michel prediction and the data in figure 8a. Comparison of Stone's static spectra with data are shown in figures 12b through 16b. The improved correlation of the Michalke and Michel flight spectra using Stone's method is primarily due to the better agreement of Stone's static prediction with data in the forward arc.

There are two differences in the way the spectra are computed using the theory of Michalke and Michel and that of the ARP-876. First the ARP-876 computes

the Strouhal number based on the relative jet velocity given by

$$St = \frac{fD}{\Delta U} \tag{46}$$

The Michalke and Michel theory, on the other hand, computes the Strouhal number based on the effective jet velocity which changes with angle and includes a correction for the stretching of the mixing region in flight. The Strouhal number for the Michalke and Michel theory is

$$St = \frac{fD}{U_e \sigma} = \frac{fD}{\Delta U} \quad \left(\frac{1 - M_f \cos\theta_o}{\sigma}\right) \tag{47}$$

The two Strouhal numbers differ only by a factor of

$$\frac{1 - M_f \cos\theta_o}{\sigma} \tag{48}$$

The effect of this factor is strongest in the forward arc while in the aft arc this factor tends toward 1 and the two Strouhal numbers are virtually identical.

Second, the theory of Michalke and Michel requires an equivalent static jet velocity which is a function of the emission angle given by

$$U_e = \frac{\Delta U}{1 - M_f \cos\theta_o} \tag{49}$$

which result is a higher jet velocity in the forward arc and lower jet velocity in the aft arc. Figure 17 shows the change in equivalent static velocity with angle for the 5 jet velocities in the data set.

This variation is required to model the ratio between the two source terms q_1 and q_2 in equation (2) correctly. According to reference 6 this is important for hot jets. However, it seems that this variation might be responsible for the poor

agreement of the Michalke and Michel flight prediction (using the ARP-876 method) for $U_j/a_o > 1.5.$ and $\theta = 150°$.

An examination of the static data at 150° indicates that as the jet velocity increases so does the high frequency content. The ARP-876 method more accurately predicts this trend than Stone's method and therefore the poor agreement of the Michalke and Michel flight prediction (using the ARP-876 method) for $U_j/a_o \geq 1.48$ is a result of the change in spectra shape with jet velocity and the reducion in the equivalent static jet velocity in the aft arc as rquired by the theory.

CONCLUSIONS

Comparison of the forward flight effects theory of A. Michalke and U. Michel with measured data have resulted in the following conclusion.

- The prediction of the ΔOASPL level by the Michalke and Michel theory for circular jets using the SAE ARP-876 method showed good agreement with data for $U_j/a_o \leq 1.5$. For this range of normalized jet velocities, a stretching parameter of $A = 1.4$ and a turbulence factor of $\sigma_1=\sigma$ are reasonable value.

- As the normalized jet velocity is increased above 1.5, the theory underpredicts the OASPL level at 90° causing the aft arc to also be underpredicted. In this range of normalized jet velocities, some enhancement of the theory is necessary.

- Comparison of the Michalke and Michel theory with measurements using the Stone method for circular jets showed the same basic trend as the comparisons using the SAE ARP-876 method.

- The use of the Michalke and Michel theory to predict the one-third octave band spectra (using the SAE ARP-876 method) will result in the flight spectra being shifted in the high frequency direction for emission angle of 30° and 60° degrees. This shift in the flight spectra is caused by the SAE ARP-876 static spectra which is also shifted toward the high frequency range for these emission angles.

- For emission angles of 90° and larger, the Michalke and Michel theory agrees very well with data (using the SAE ARP-876 method) for $U_j/a_o \leq 1.5$. When the normalized jet velocity is increased above 1.5, the shape of the flight spectra for $\theta_o = 150°$ is incorrectly predicted. The difficulty is attributed to the reduction in the equivalent static jet velocity in the aft arc, which is required by the theory to properly model the ratio of the two source terms q_1 and q_2.

- The use of the Michalke and Michel theory to predict the one-third octave band spectra (using the Stone method) will result in good agreement with data at all angles and $U_j/a_o \leq 1.5$.

- Finally, the Michalke and Michel theory was also compared with measurements from a coaxial jet where the static prediction base was the Stone coaxial method. The prediction of the OASPL level showed very good results in those cases where airframe noise was not a factor.

REFERENCES

1. Lighthill, M. J.: On Sound Generated Aerodynamically II. Turbulence as a Source of Sound. Proceedings of the Royal Society, A211, 1954, pp. 1-21.

2. Ffowcs-Williams, J. E.: The Noise From Turbulence Convected at High Speed. Phil. Trans. Roy. Soc. London, ser. A, vol. 255, no. 1061, Apr. 18, 1963, pp. 469-503.

3. Amiet, R. K.: Correction of Open Jet Wind Tunnel Measurements for Shear Layer Refraction. AIAA paper 75-536, 1975.

4. Drevet, P.; Duponchel, J. P.; and Jacques, J. R.: The Effect of Flight on Jet Noise as Observed on the Bertin Aerotrain. J. Sound & Vib., vol. 54, no. 2, Sept. 22, 1977, pp. 173-201.

5. Michalke, A.; and Michel, U.: Relation Between Static and In-Flight Directivities of Jet Noise. J. Sound & Vib., vol. 63, no. 4, Apr. 22, 1979, pp. 602-605.

6. Michalke A.; and Michel, U.: Prediction of Jet Noise in Flight From Static Tests. J. Sound & Vib., vol. 67, no. 3, Dec. 8, 1979, pp. 341-367.

7. Michalke, A.; and Michel, U.: Prediction of Flyover Noise From Single and Coannular Jets. AIAA-80-1031, June 1980.

8. Michel, U.; and Michalke, A.: Prediction of Flyover Jet Noise Spectra From Static Tests. NASA TM-83219, 1981.

9. Gas Turbine Jet Exhaust Noise Prediction. ARP-876, Soc. Automot. Eng., Mar. 1978. (Supersedes AIR 876.)

10. Hoch, R. G.; Duponchel, J. P.; Cocking, B. J.; and Bryce, W. D.: Studies on the Influence of Density on Jet Noise. SNECMA and NGTE paper presented at the First International Symposium on Air Breathing Engines (Marseille, France), June 19-23, 1972.

11. Stone, J. R.; and Montegani, F. J.: An Improved Prediction Method for the Noise Generated in Flight by Circular Jets. NASA TM-81470, 1980.

12. Michalke, A.; and Hermann, G.: On the Inviscid Instability of a Circular Jet With External Flow. J. Fluid Mech., vol. 114, Jan. 1982, pp. 343-359.

13. Morse, P. M. and Ingard, K. U.: Theoretical Acoustics. New York, McGraw-Hill Book Company, 1968.

14. Szewcyk, V.M.: Coaxial Jet Noise in Flight. AIAA 79-0636, 1979.

TABLE I

Jet Noise and Forward Flight Effects Methods
used by ICAO Committee Members

Participant	Jet Noise Prediction Method
NASA-ANOPP	ARP-876 plus own modified; Hoch SAE flight exponent.
SNECMA	ARP-876 plus own modified; Hoch SAE flight exponent.
British Aerospace Corp.	ARP-876 (pre-publication) plus SAE Hoch Proposal.
The Boeing Co.	ARP-876 plus own flight exponent.
McDonnell Douglas Corp.	Own method.
Lockheed Corp.	Modified ARP-876.
Pratt & Whitney Aircraft Group	ARP-876 plus near average Hoch.
General Electric Co.	ARP-876 plus 1 dB plus Bushell flight exponent.
Rolls-Royce Limited	ARP-876 plus modified Hoch flight exponent.

TABLE II

Forward Flight Index, $m(\theta)$
for Single Stream Circular Jets

Directivity Angle θ, degrees	Forward Flight Index, $m(\theta)$
0	3.0
10	1.65
20	1.1
30	0.5
40	0.2
50	0.
60	0.
70	0.1
80	0.4
90	1.0
100	1.9
110	3.0
120	4.7
130	7.0
140	8.5
150	8.5
160	8.5
170	8.5
180	8.5

TABLE III

Operating Condition for Bertin Aerotrain Data (Circular Jet)

Case No.	U_j/a_o	M_f	T_j/T_a	P_j/P_a
1	1.09	.24	2.64	1.38
2	1.29	.24	2.74	1.57
3	1.48	.24	2.86	1.79
4	1.63	.24	3.01	1.97
5	1.84	.24	3.76	2.22

TABLE IV

Operating Conditions for RB-211 Data (Coaxial Jet)

Case No.	U_c/a_o	U_b/a_o	M_f	T_c/T_a	T_b/T_a
1	1.15	.85	.51	2.74	1.15
2	.87	.66	.27	2.55	1.08
3	1.28	.91	.50	2.93	1.16
4	1.07	.75	.27	2.71	1.11
5	1.25	.83	.27	2.93	1.13

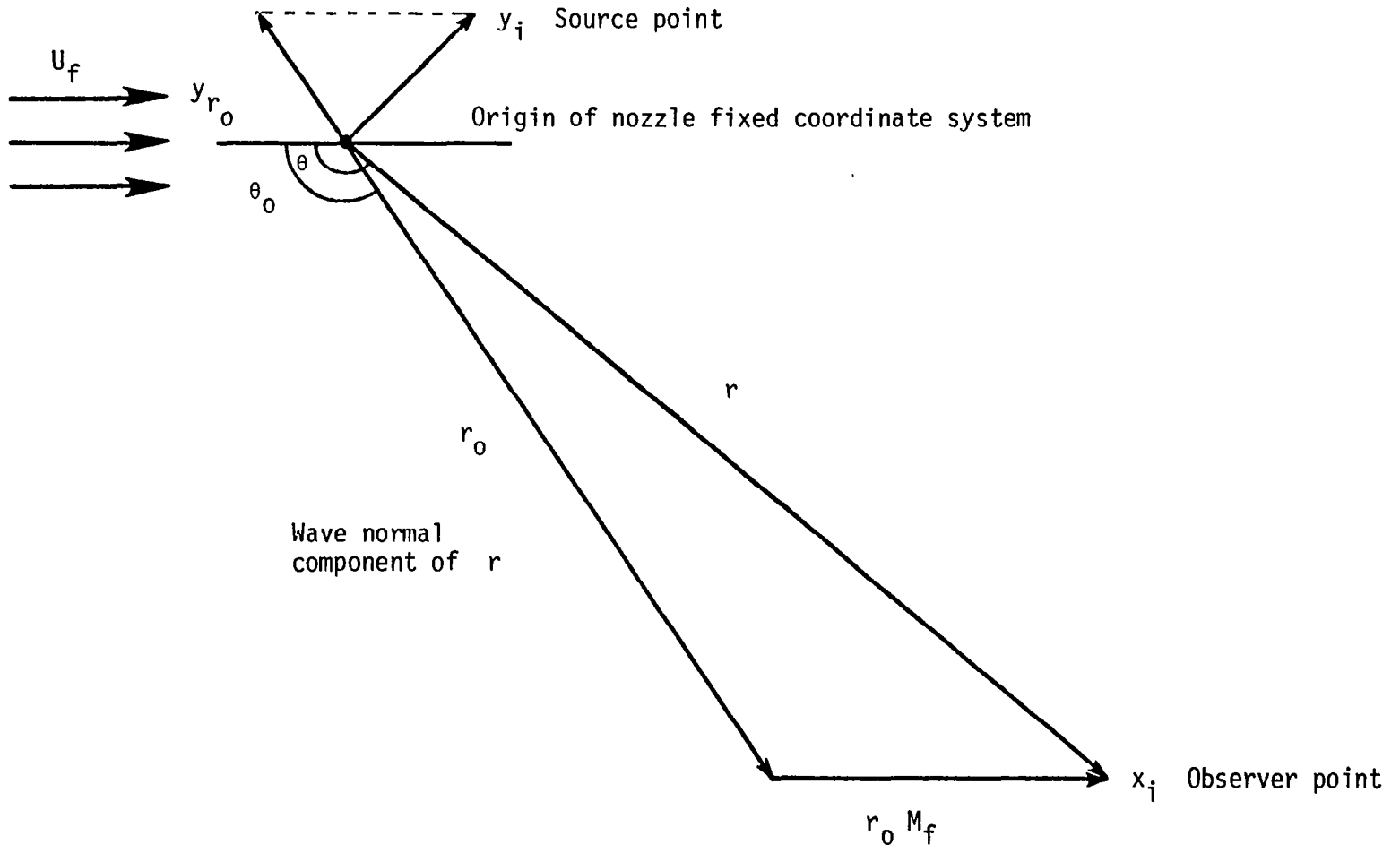

Figure 1. - Relation between observer angle θ, observer distance r, emission angle θ_o and wave normal distance r_o for a source in a moving stream.

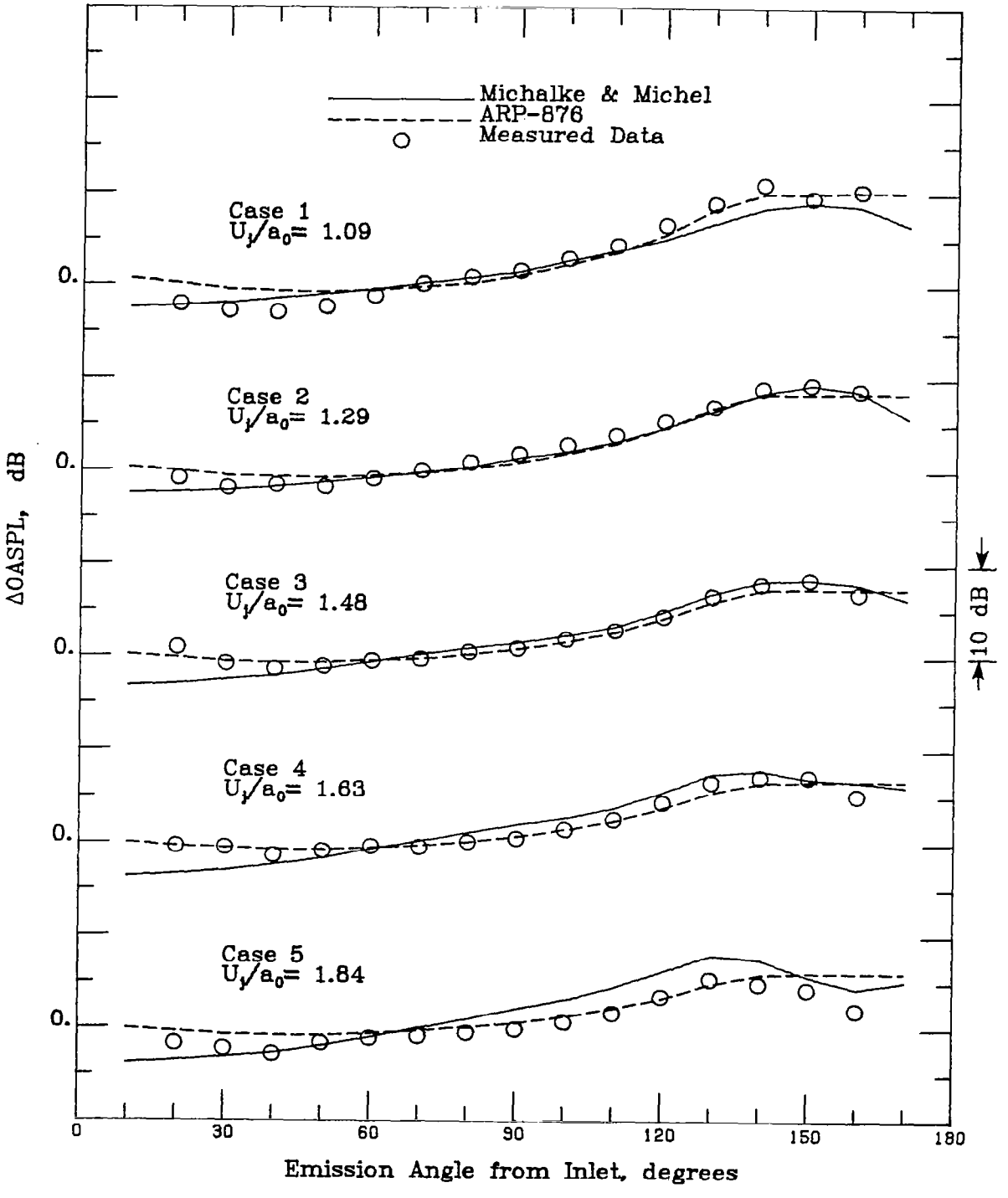

Figure 2. - Comparison of jet noise reduction levels from ref. 4 with prediction using the Michalke and Michel theory (eq. 25) and the ARP-876 prediction (eq. 29). M_f = .24 A = 1.4 $\sigma_1 = \sigma$.

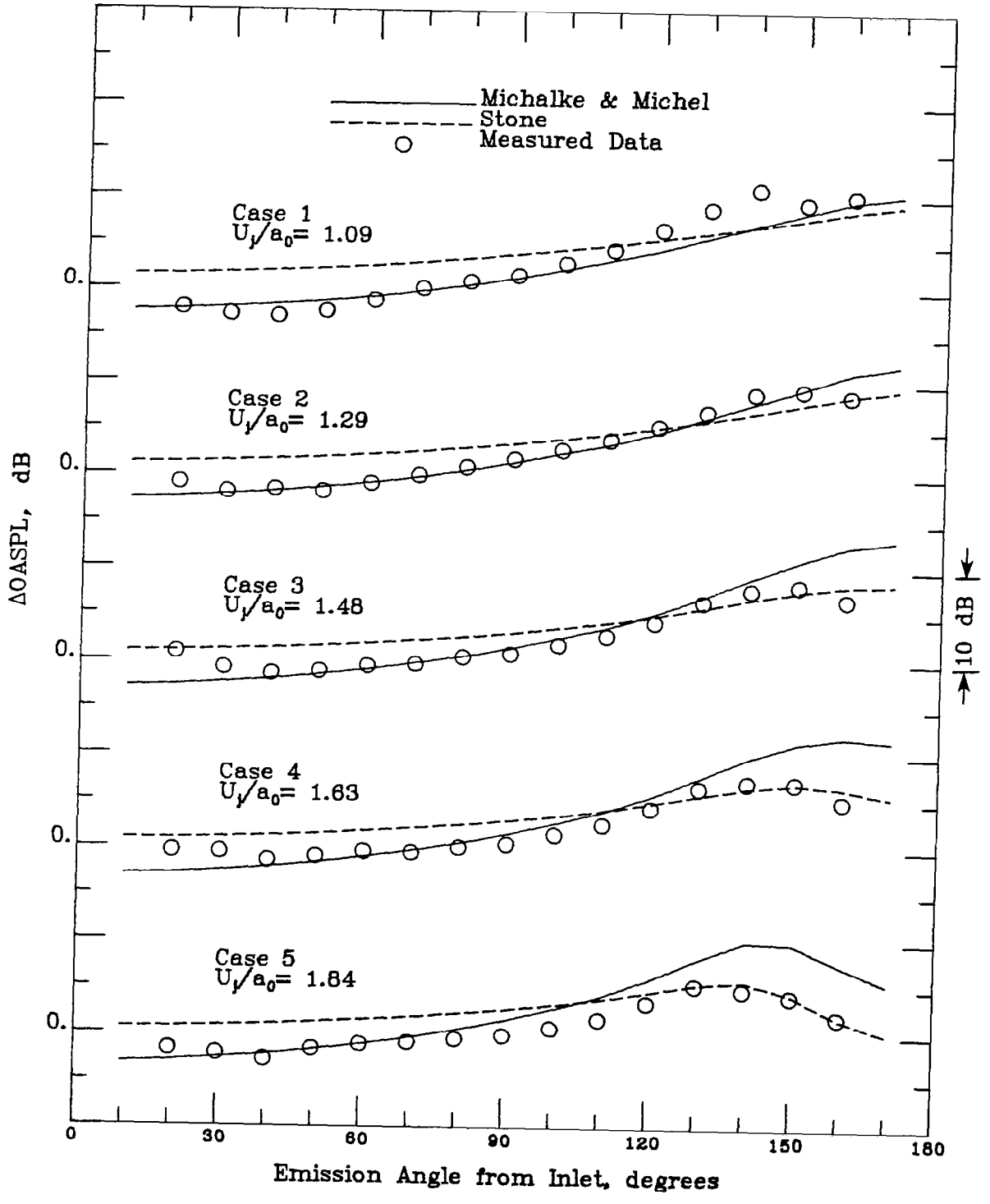

Figure 3. - Comparison of jet noise reduction levels from ref. 4 with prediction using the Michalke and Michel theory (eq. 25) and Stone's prediction method (eq. 31). M_f = .24 A = 1.4 $\sigma_1 = \sigma$.

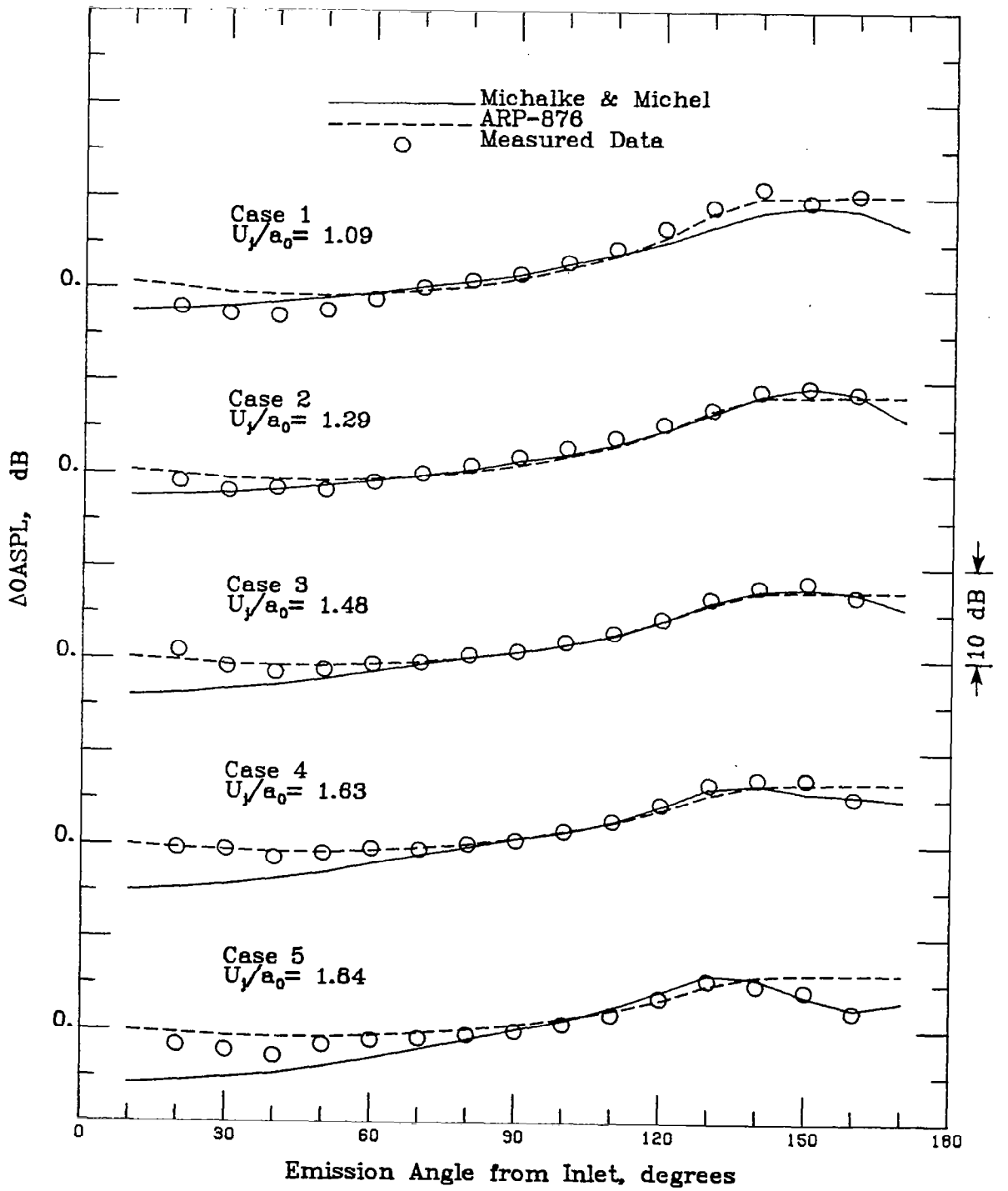

Figure 4. - Jet noise reduction levels with Michalke and Michel prediction adjusted to match data at 90° in cases 3, 4 and 5.

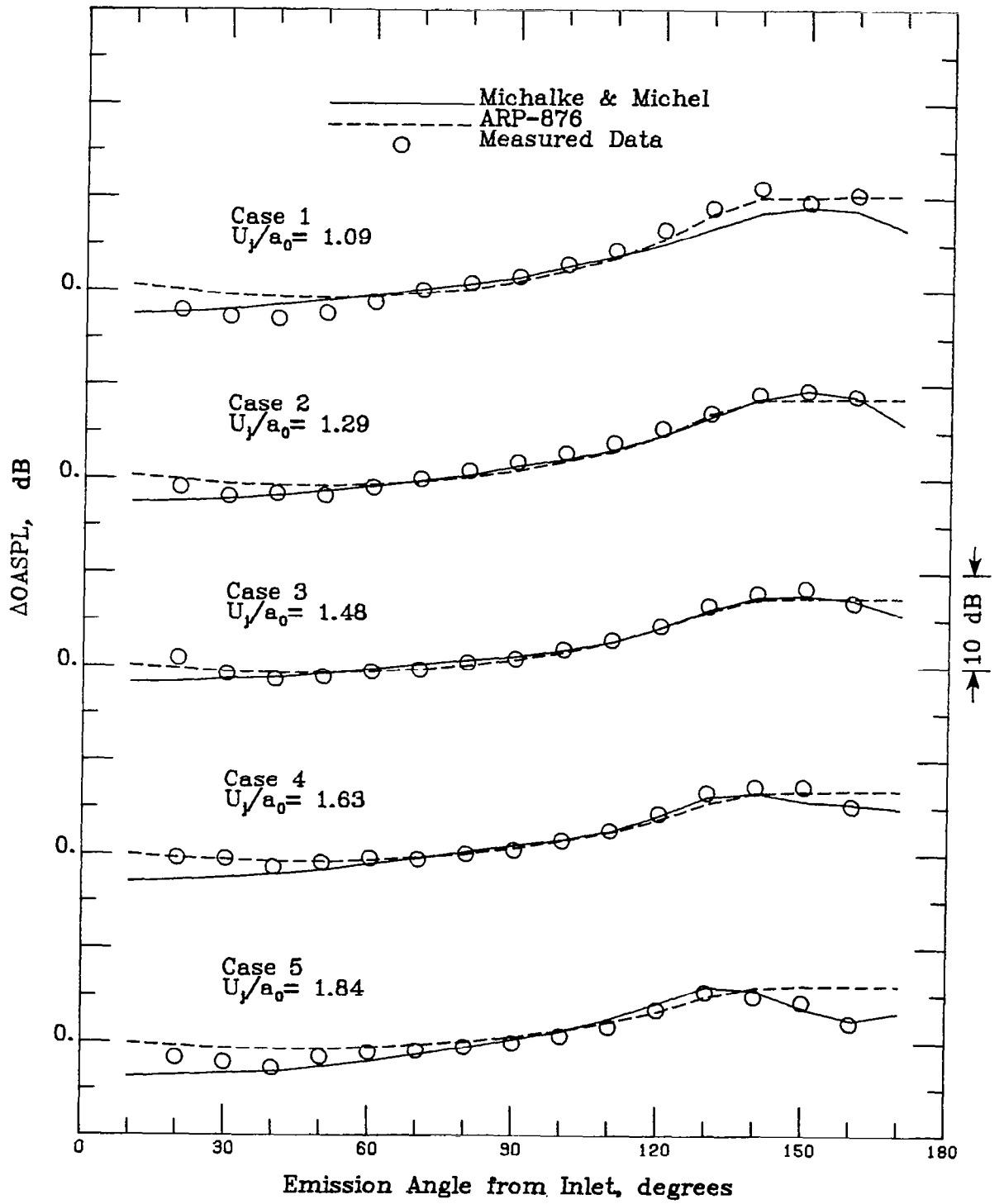

Figure 5. - Jet noise reduction levels with Michalke and Michel prediction adjusted to match data at 90° and forward arc correction (eq. 43) applied to cases 3, 4 and 5.

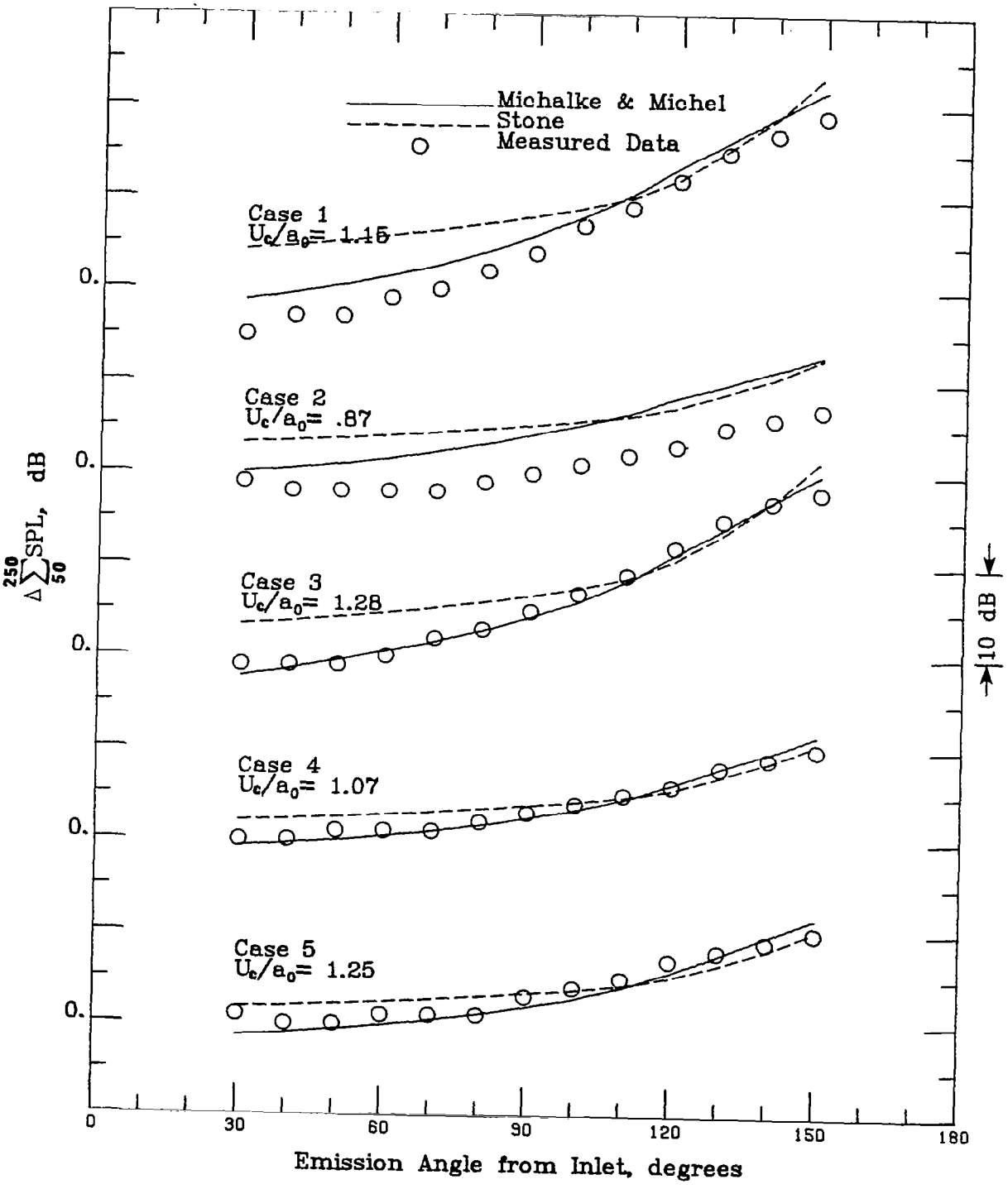

Figure 6. - Comparison of coaxial jet noise prediction levels from ref. 14 with prediction using the Michalke and Michel theory and Stone's prediction method.

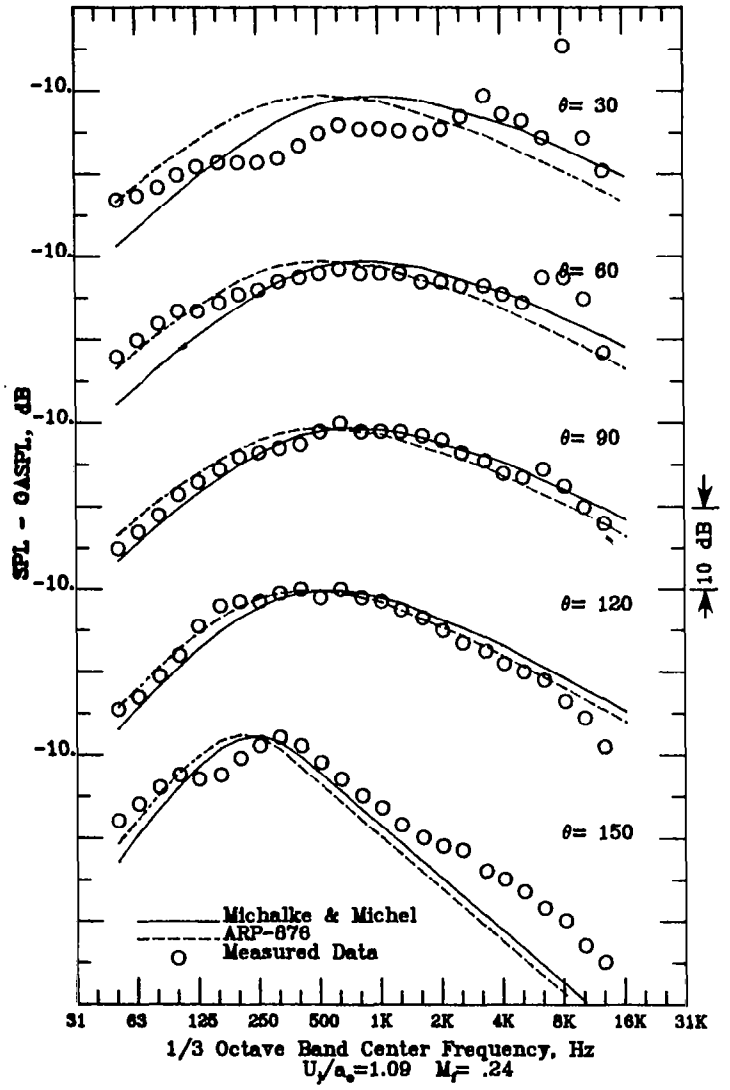

Figure 7a. - Comparison of in-flight relative 1/3 octave band spectra from ref. 4 with prediction using the Michalke and Michel theory (eq. 25) and the ARP-876 prediction (refs. 9 and 10).

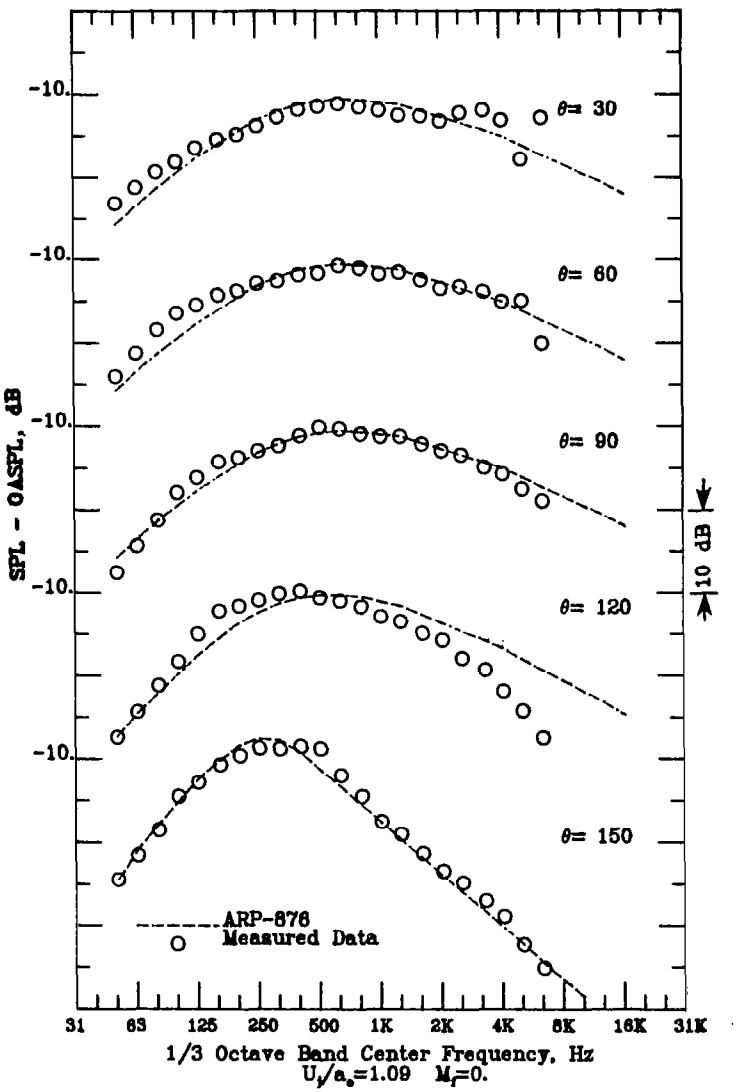

Figure 7b. - Comparison of static relative 1/3 octave band spectra from ref. 4 and the ARP-876 static prediction (ref. 9).

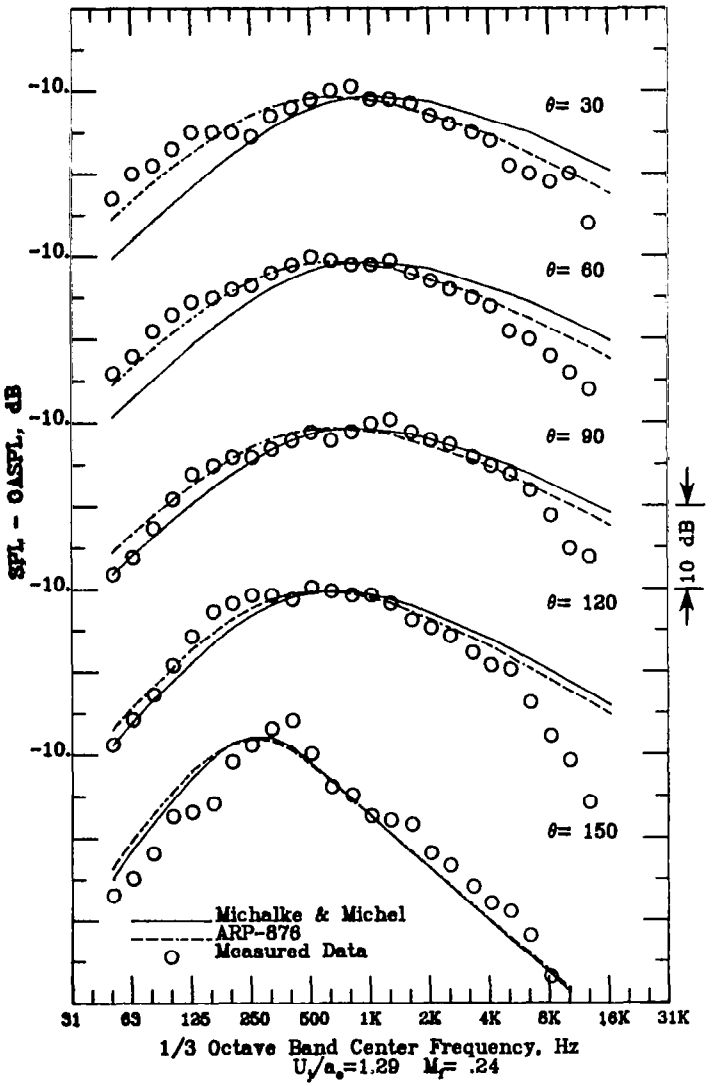

Figure 8a. - Comparison of in-flight relative 1/3 octave band spectra from ref. 4 with prediction using the Michalke and Michel theory (eq. 25) and the ARP-876 prediction (refs. 9 and 10).

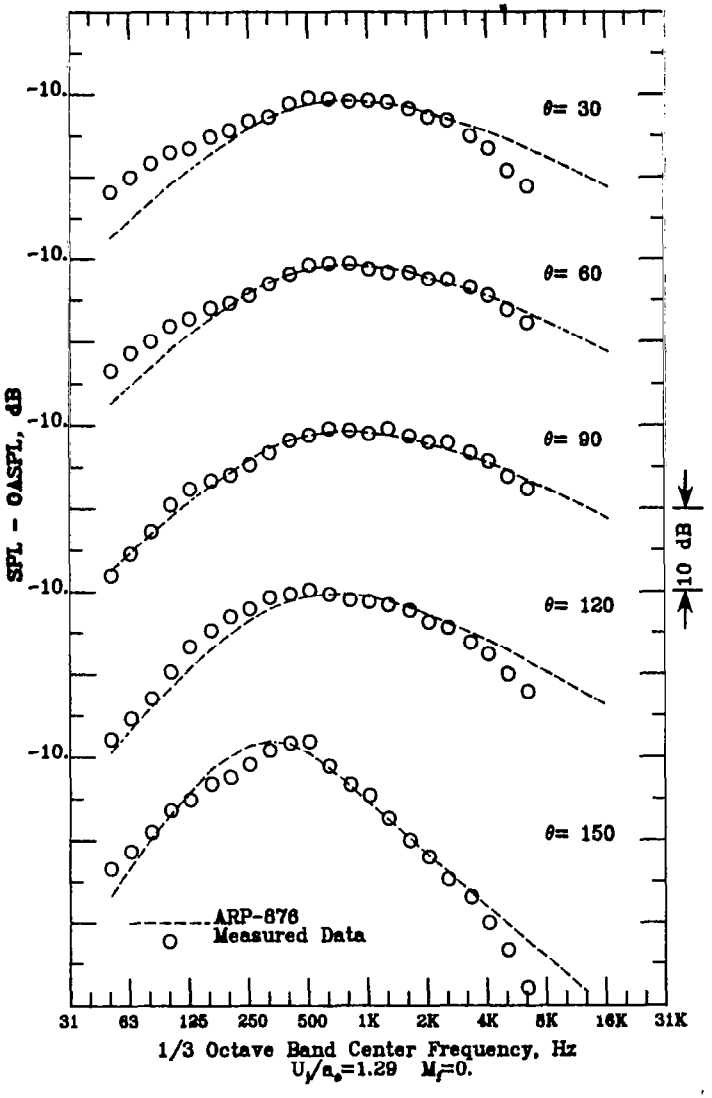

Figure 8b. - Comparison of static relative 1/3 octave band spectra from ref. 4 and the ARP-876 static prediction (ref. 9).

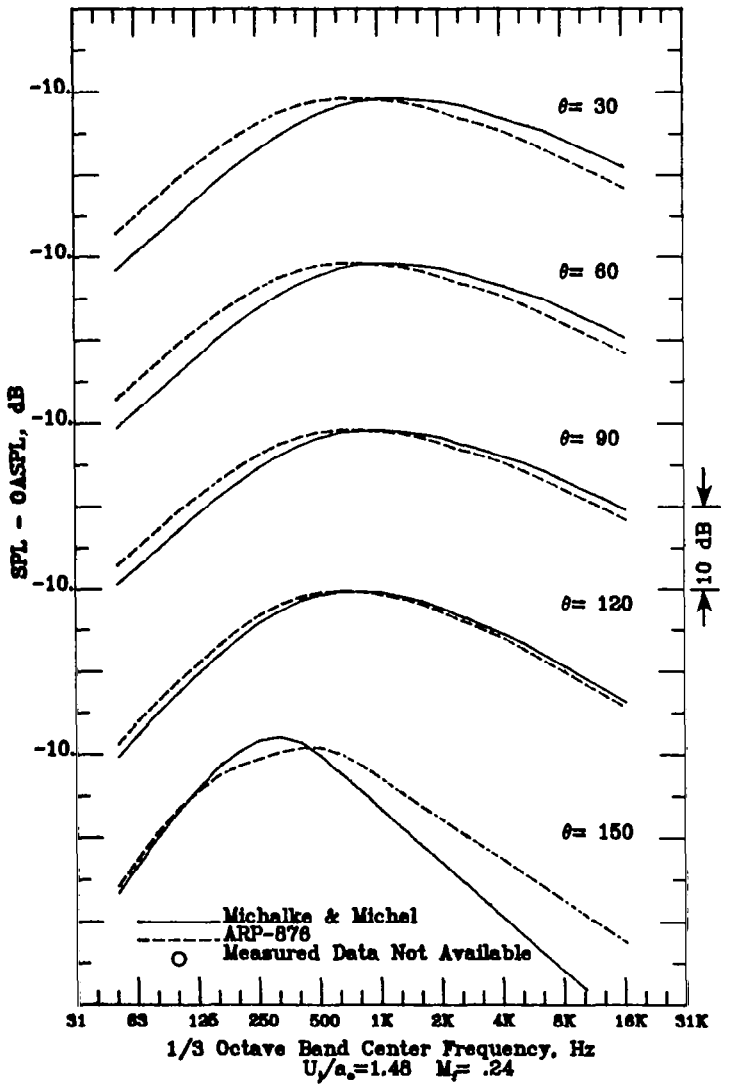

Figure 9a. - Comparison of in-flight relative 1/3 octave band spectra using the Michalke and Michel theory (eq. 25) and the ARP-876 prediction (refs. 9 and 10).

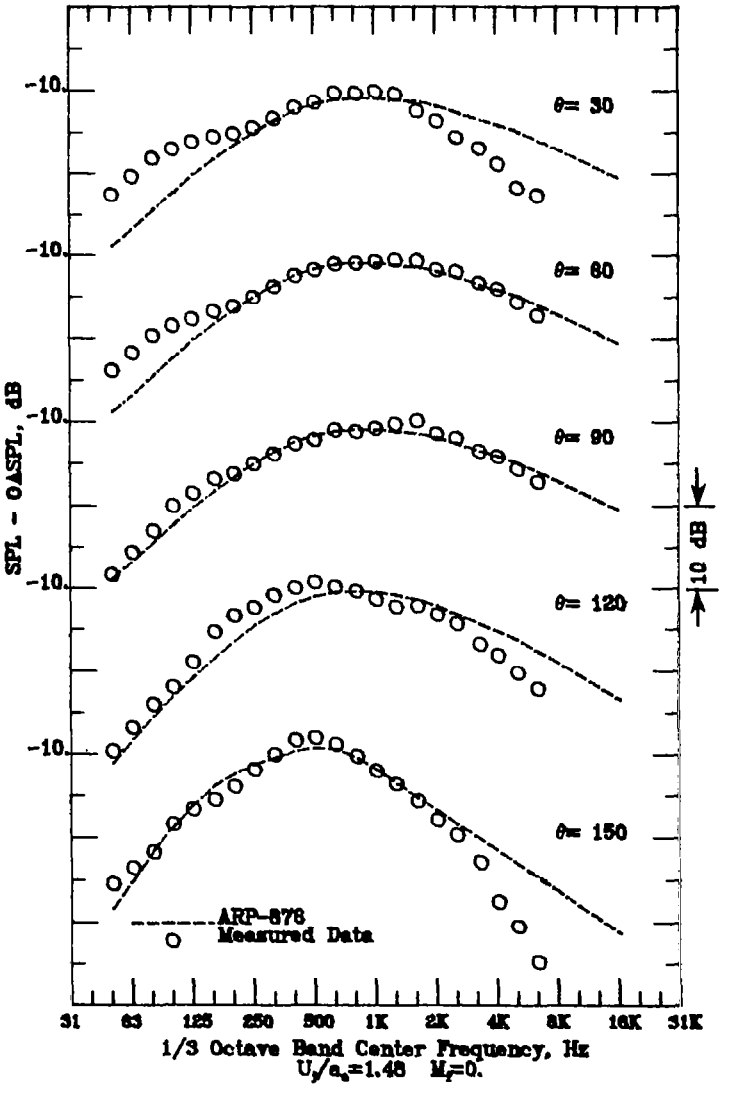

Figure 9b. - Comparison of static relative 1/3 octave band spectra from ref. 4 and the ARP-876 static prediction (ref. 9).

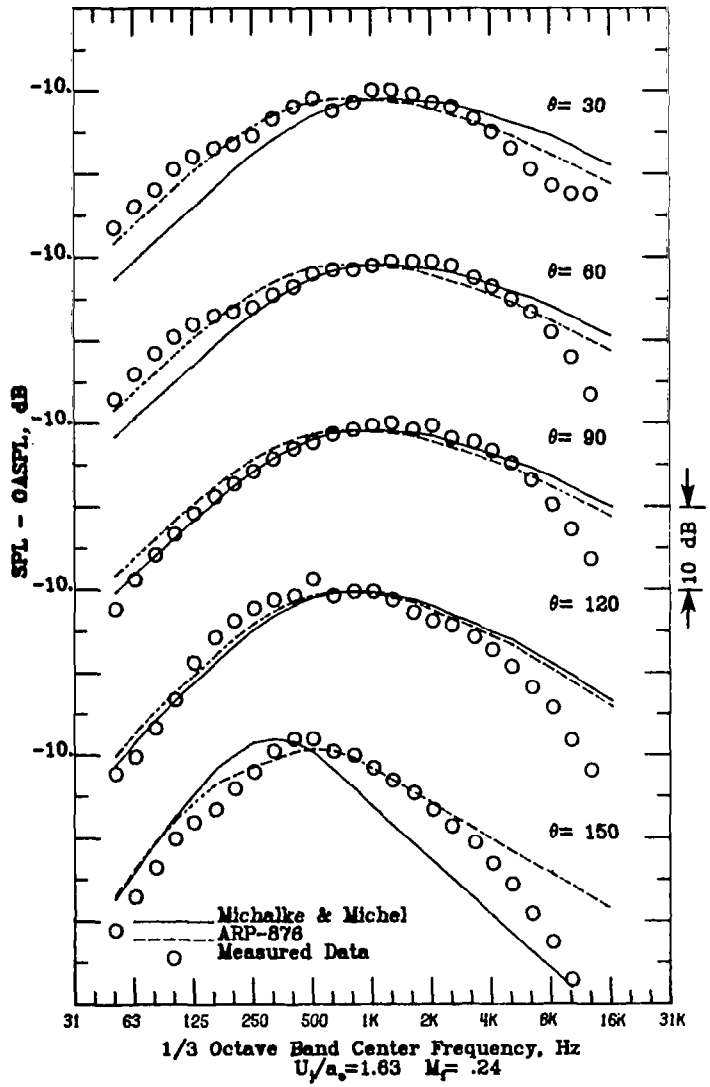

Figure 10a.- Comparison of in-flight relative 1/3 octave band spectra from ref. 4 with prediction using the Michalke and Michel theory (eq. 25) and the ARP-876 prediction (refs. 9 and 10).

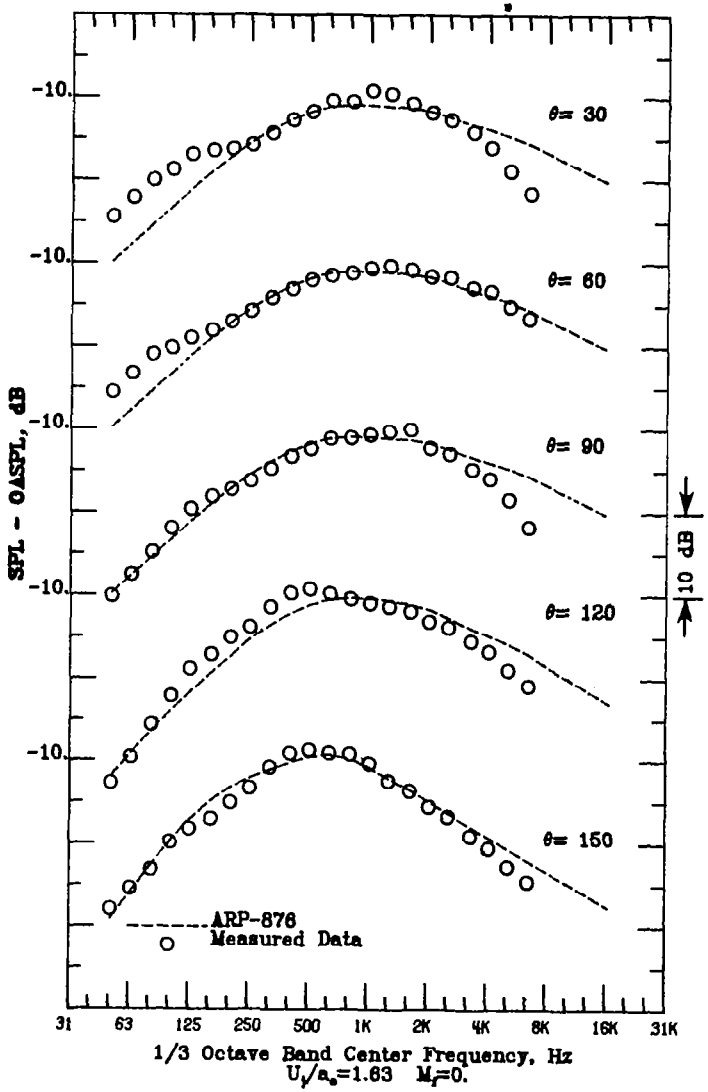

Figure 10b.- Comparison of static relative 1/3 octave band spectra from ref. 4 and the ARP-876 static prediction (ref. 9).

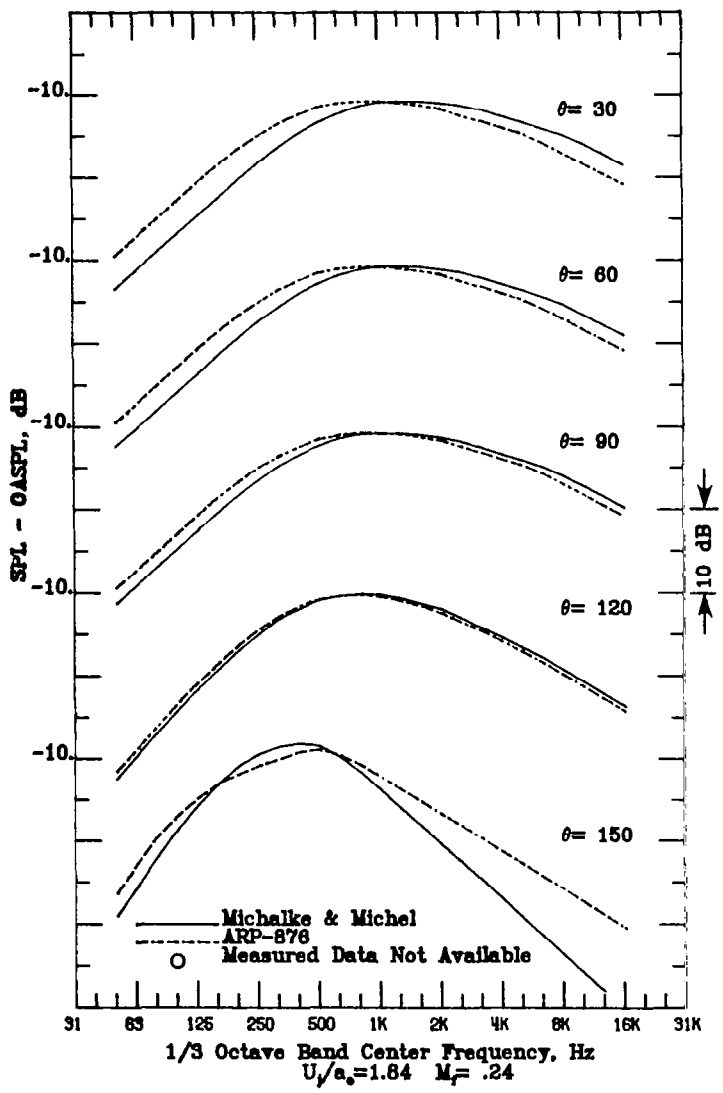

Figure 11a.- Comparison of in-flight relative 1/3 octave band spectra using the Michalke and Michel theory (eq. 25) and the ARP-876 prediction (refs. 9 and 10).

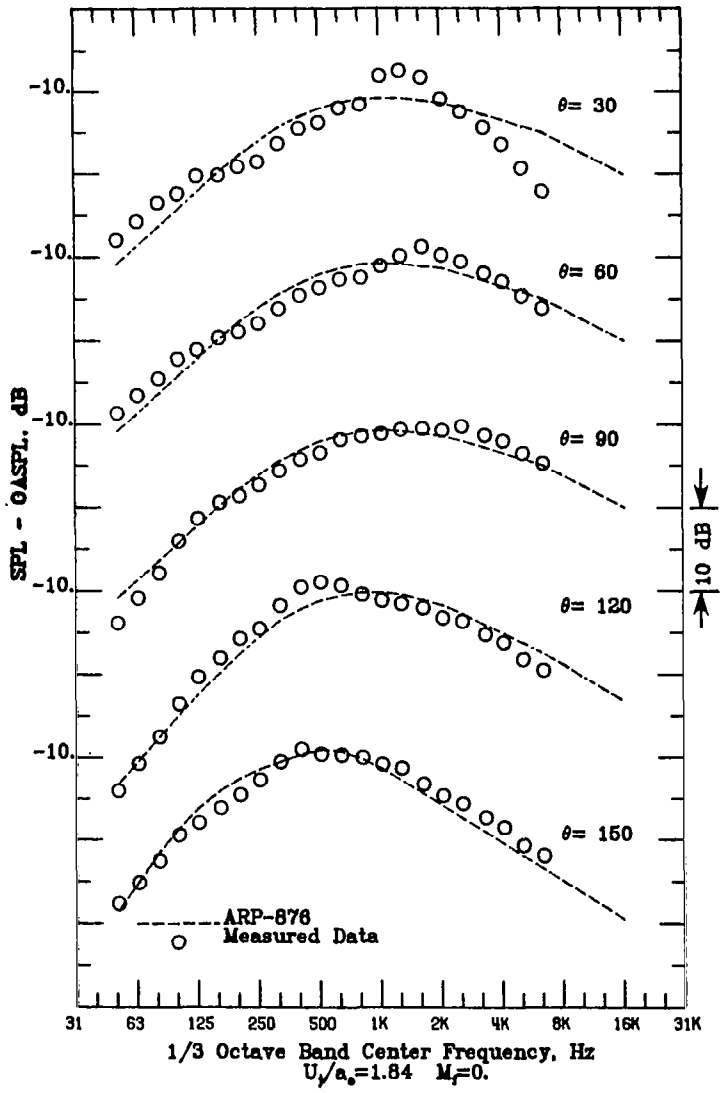

Figure 11b.- Comparison of static relative 1/3 octave band spectra from ref. 4 and the ARP-876 static prediction (ref. 9).

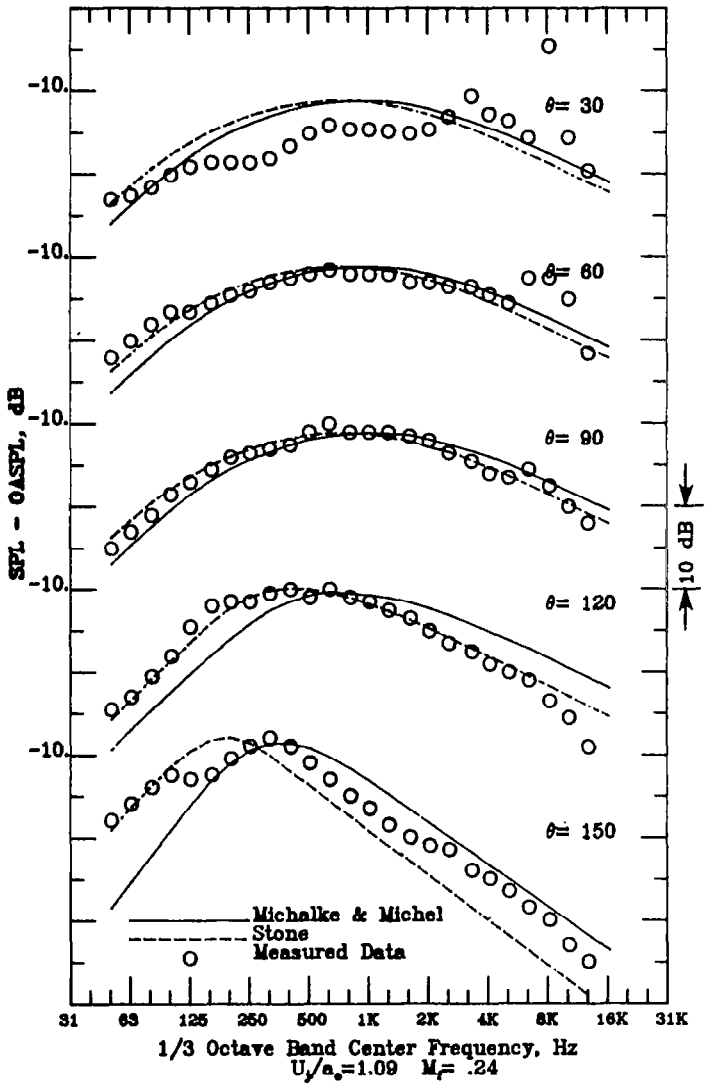

Figure 12a.- Comparison of in-flight relative 1/3 octave band spectra from ref. 4 with prediction using the Michalke and Michel theory (eq. 25) and Stone's method (ref. 11).

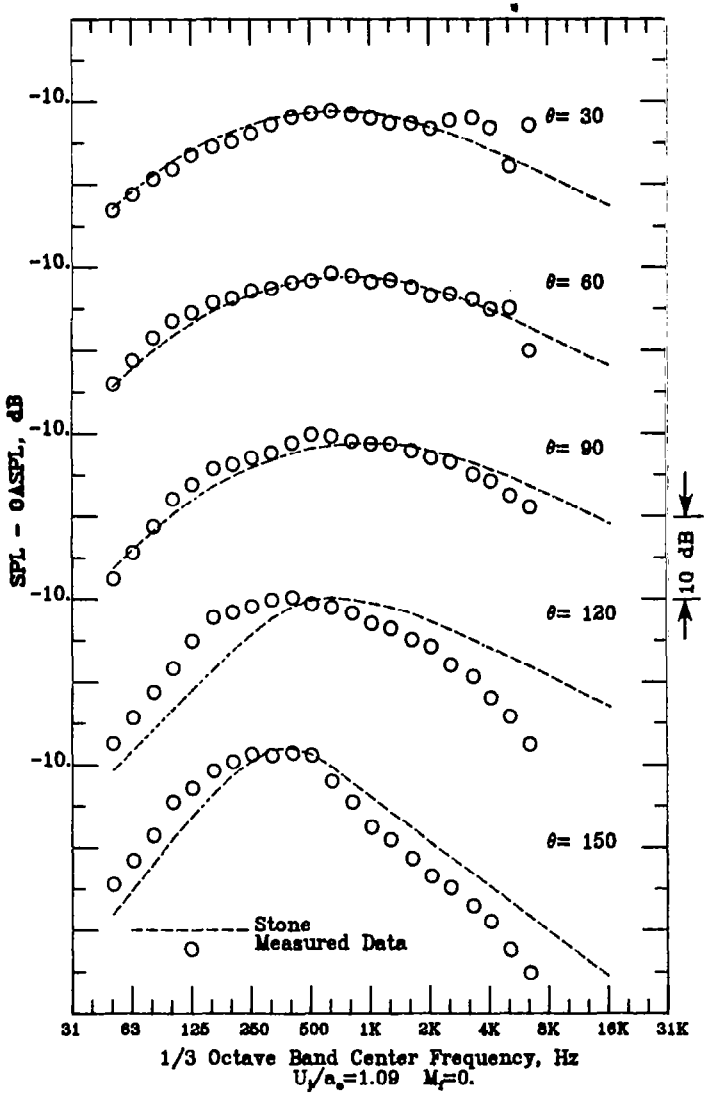

Figure 12b.- Comparison of static relative 1/3 octave band spectra from ref. 4 and Stone's static prediction (ref. 11).

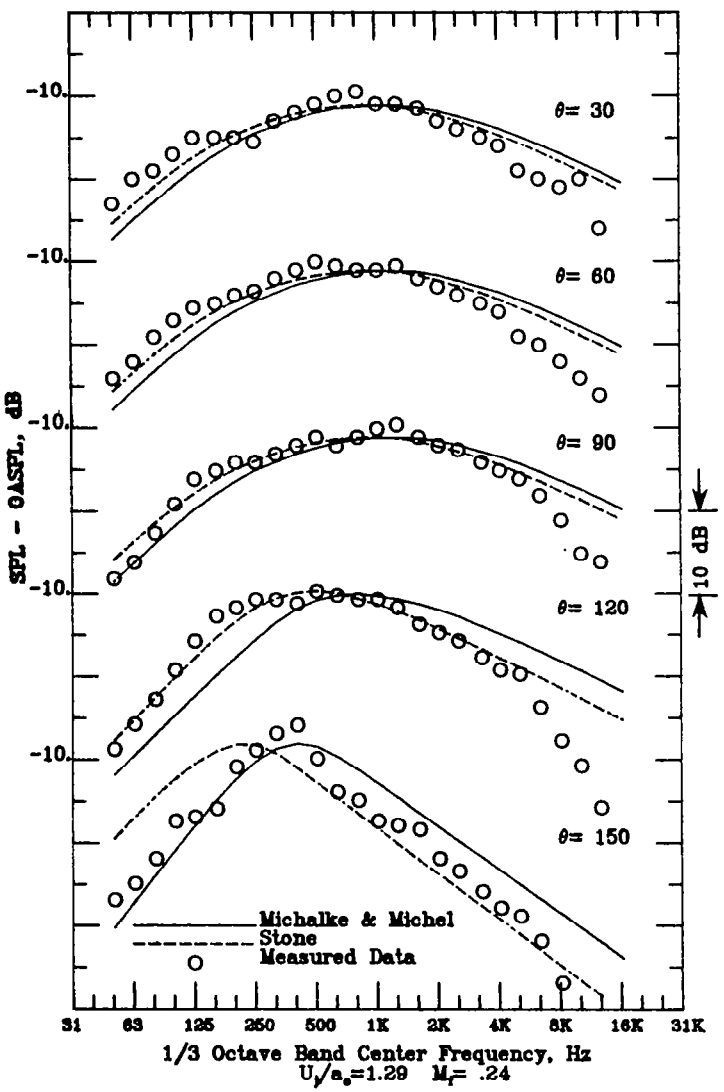

Figure 13a.- Comparison of in-flight relative 1/3 octave band spectra from ref. 4 with prediction using the Michalke and Michel theory (eq. 25) and Stone's method (ref. 11).

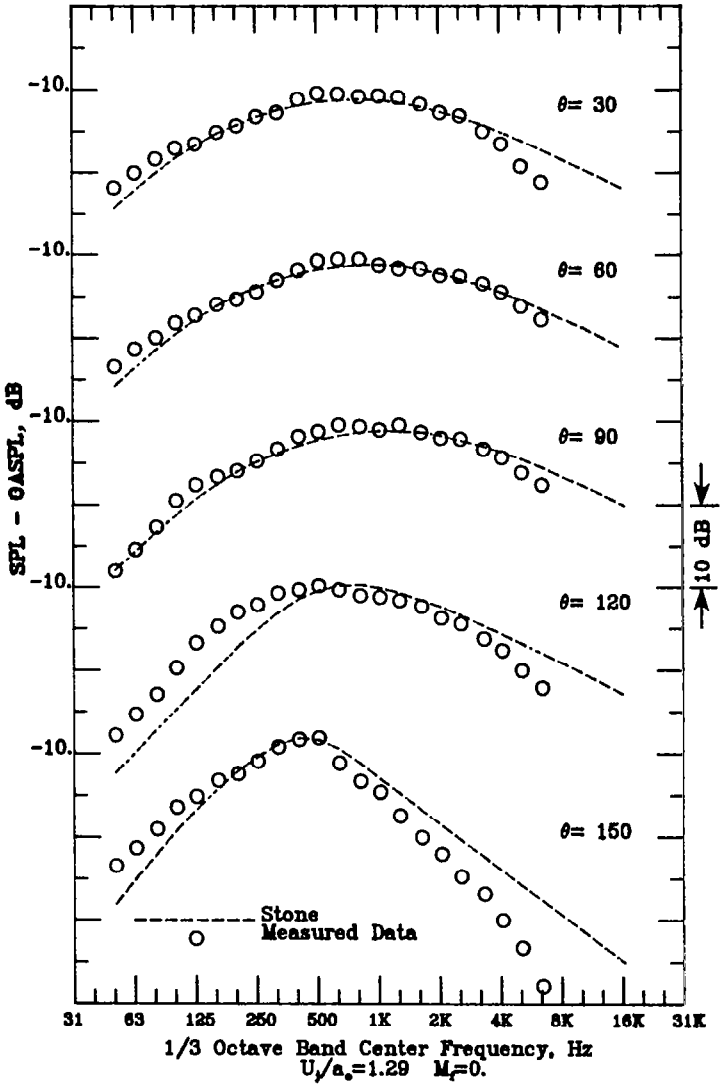

Figure 13b.- Comparison of static relative 1/3 octave band spectra from ref. 4 and Stone's static prediction (ref. 11).

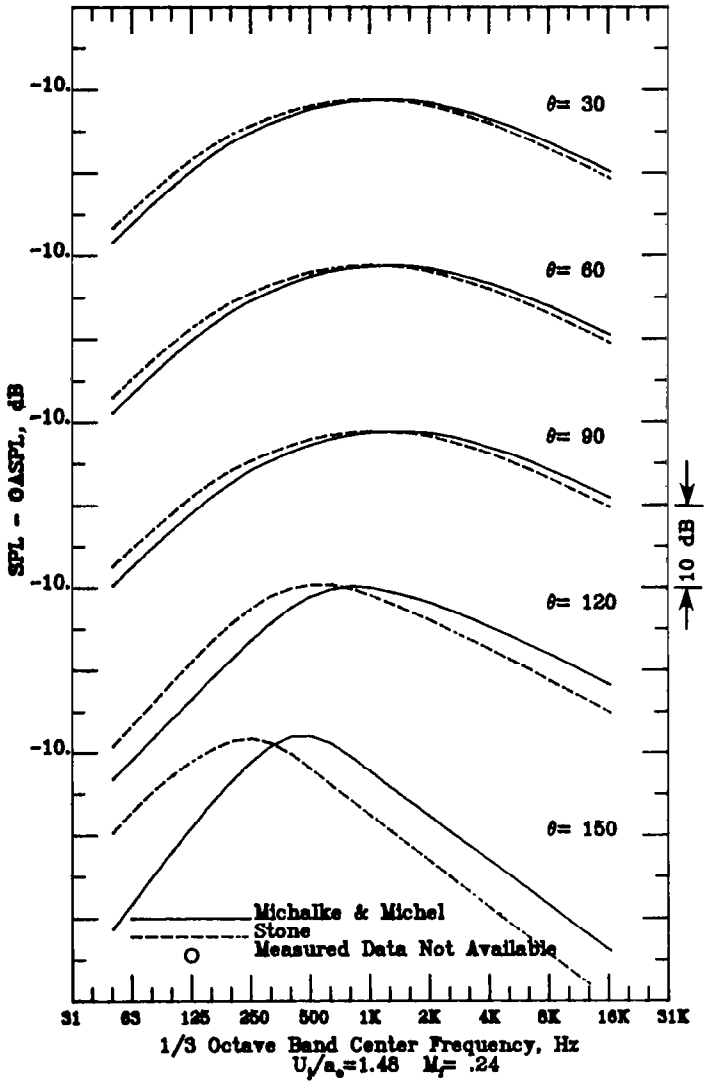

Figure 14a.- Comparison of in-flight relative 1/3 octave band spectra using the Michalke and Michel theory (eq. 25) and Stone's method (ref. 11).

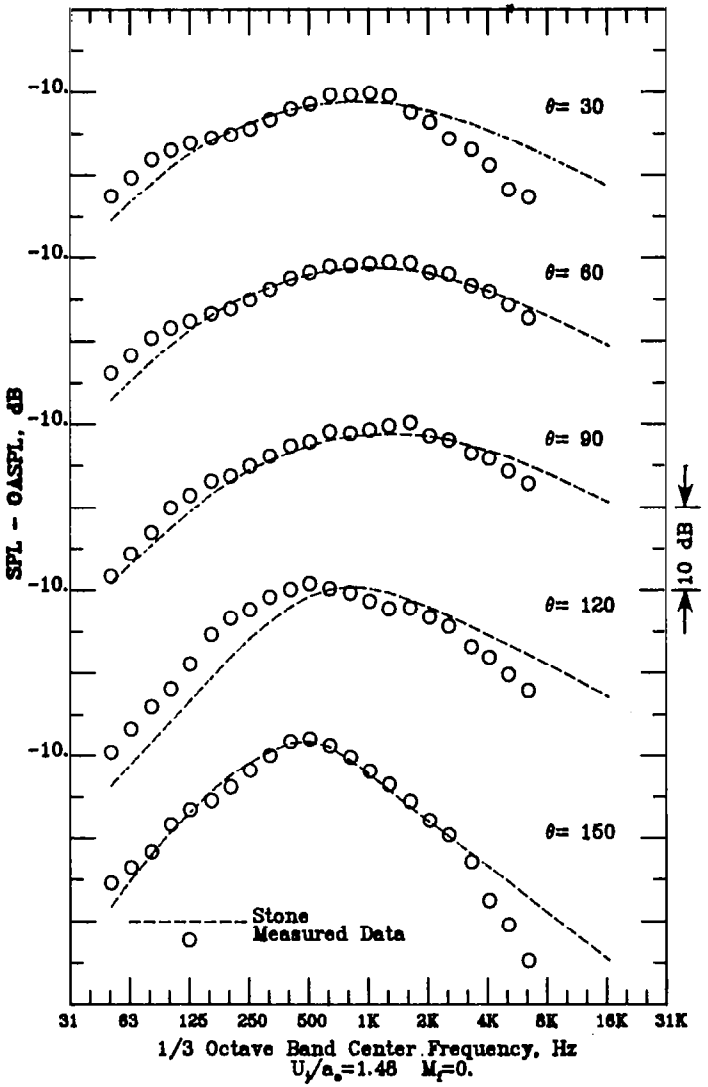

Figure 14b.- Comparison of static relative 1/3 octave band spectra from ref. 4 and Stone's static prediction (ref. 11).

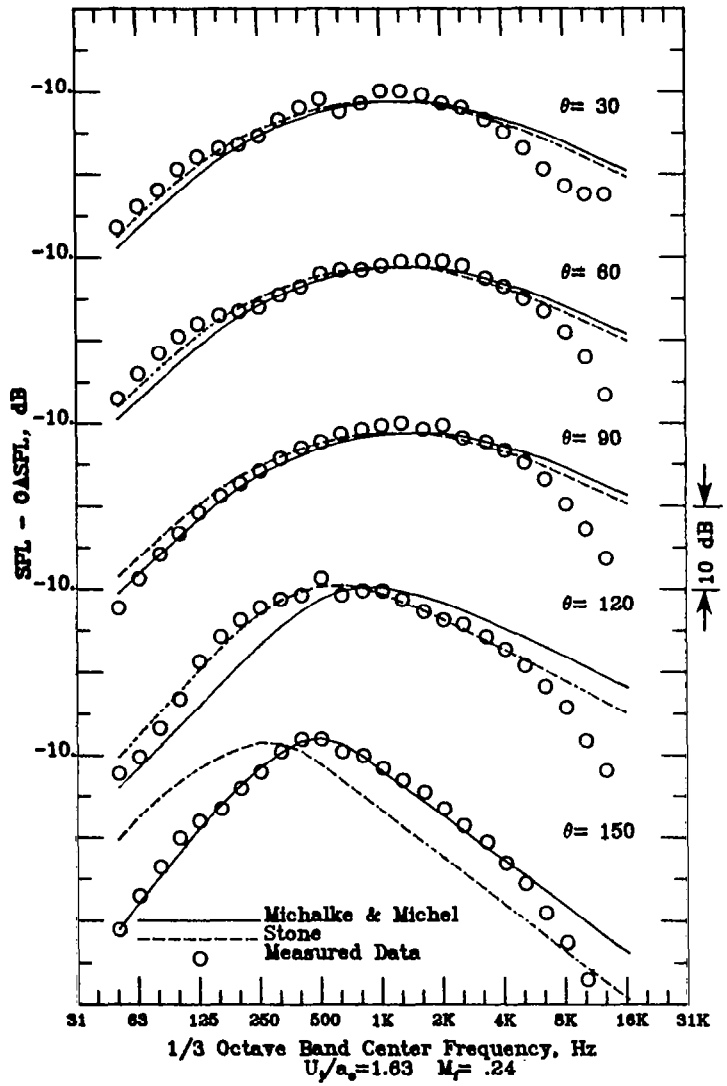

Figure 15a.- Comparison of in-flight relative 1/3 octave band spectra from ref. 4 with prediction using the Michalke and Michel theory (eq. 25) and Stone's method (ref. 11).

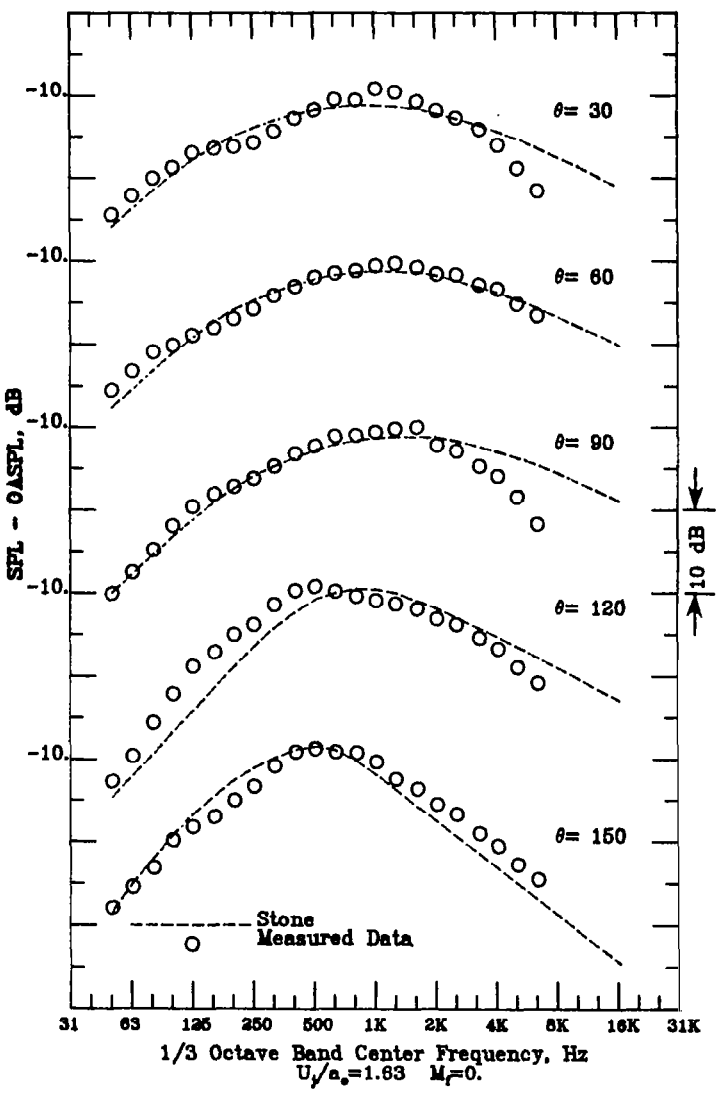

Figure 15b.- Comparison of static relative 1/3 octave band spectra from ref. 4 and Stone's static prediction (ref. 11).

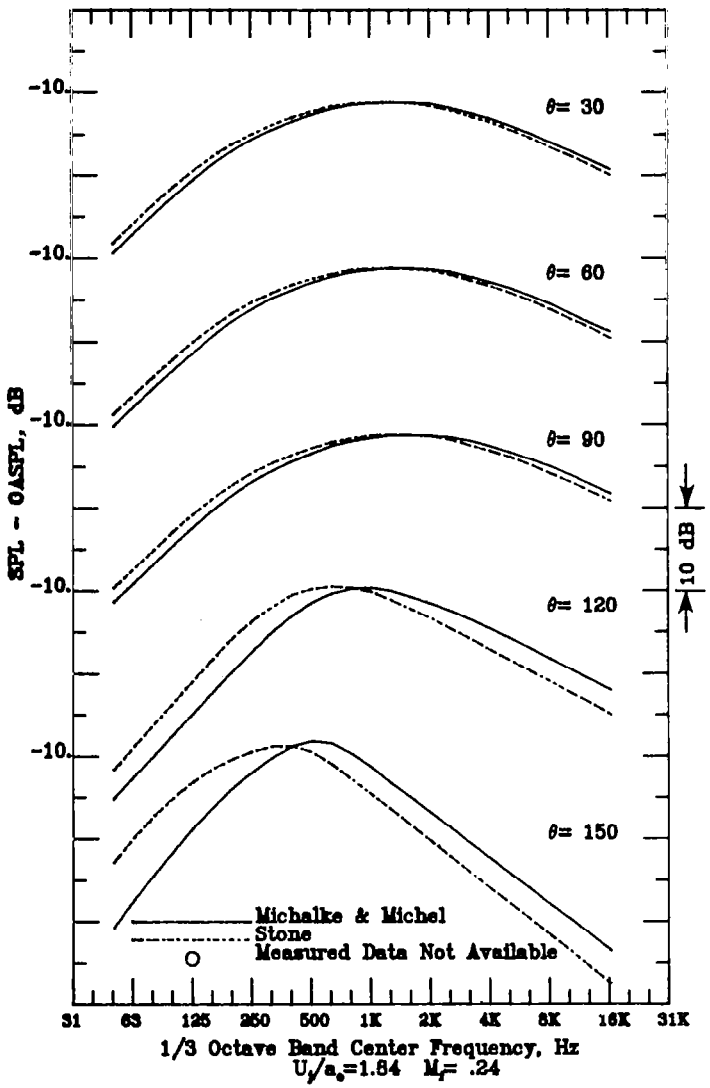

Figure 16a.- Comparison of in-flight relative 1/3 octave band spectra using the Michalke and Michel theory (eq. 25) and Stone's method (ref. 11).

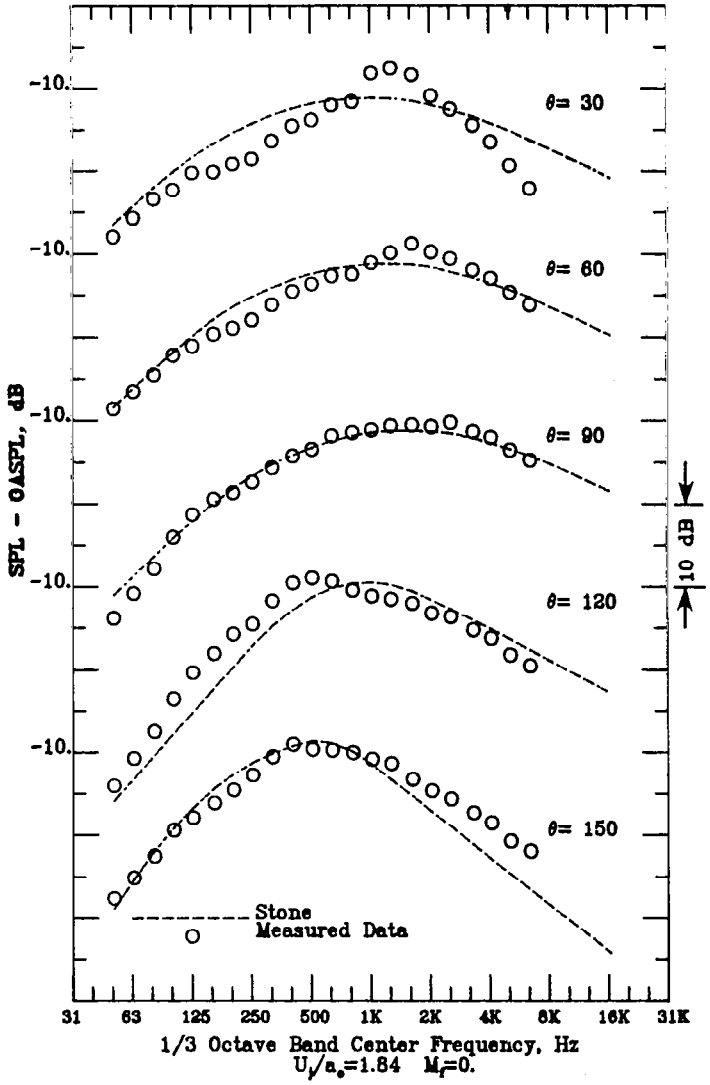

Figure 16b.- Comparison of static relative 1/3 octave band spectra from ref. 4 and Stone's static prediction (ref. 11).

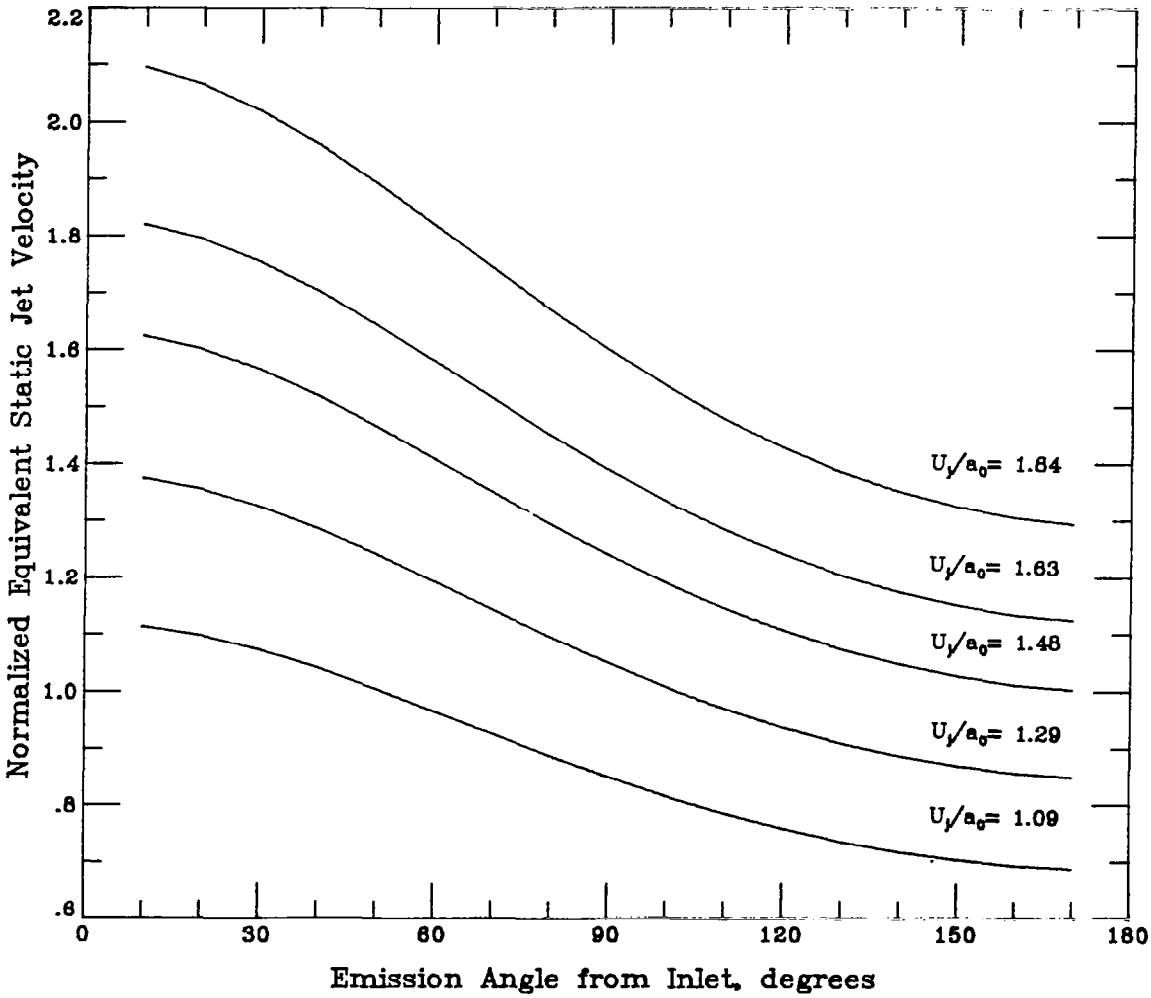

Figure 17. - Equivalent static jet velocity as a function of emission angle (eq. 9) for the five Bertin Aerotrain test cases. M_f = .24.

1. Report No.	2. Government Accession No.	3. Recipient's Catalog No.
NASA CR-3665		

4. Title and Subtitle	5. Report Date
COMPARISON OF FORWARD FLIGHT EFFECTS THEORY OF A. MICHALKE AND U. MICHEL WITH MEASURED DATA	January 1983
	6. Performing Organization Code

7. Author(s)	8. Performing Organization Report No.
John W. Rawls, Jr.	
	10. Work Unit No.

9. Performing Organization Name and Address	11. Contract or Grant No.
Kentron International, Inc. Kentron Technical Center 3221 North Armistead Avenue Hampton, Virginia 23666	NAS1-16000
	13. Type of Report and Period Covered
12. Sponsoring Agency Name and Address	Contractor Report
National Aeronautics and Space Administration Washington, D. C. 20546	14. Sponsoring Agency Code

15. Supplementary Notes

Langley Technical Monitor: William E. Zorumski
Final Report

16. Abstract

The scaling laws of A. Michalke and U. Michel predict flyover noise of a single stream shock free circular jet from static data or static predictions. The theory is based on a farfield solution to Lighthill's equation and includes density terms which are important for heated jets. This theory is compared with measured data using two static jet noise prediction methods. The comparisons indicate the theory yields good results when the static noise levels are accurately predicted.

17. Key Words (Suggested by Author(s))	18. Distribution Statement
Flight Effects Jet Noise Aeroacoustics	Unclassified - Unlimited Subject Category 71

19. Security Classif. (of this report)	20. Security Classif. (of this page)	21. No. of Pages	22. Price
Unclassified	Unclassified	54	A04

For sale by the National Technical Information Service, Springfield, Virginia 22161

NASA-Langley, 1983